Correlating sparse sensing for network-wide traffic speed estimation: An integrated graph tensor-based kriging approach

Tong Nie^a, Guoyang Qin^a, Yunpeng Wang^b, Jian Sun^{a,*}

^aDepartment of Traffic Engineering & Key Laboratory of Road and Traffic Engineering, Ministry of Education, Tongji University, Shanghai 201804, China ^b Beijing Key Laboratory for Cooperative Vehicle Infrastructure Systems and Safety Control, School of Transportation Science and Engineering, Beihang University, Beijing 100191, China

Abstract

Traffic speed is central to characterizing the fluidity of the road network. Many transportation applications rely on it, such as real-time navigation, dynamic route planning, and congestion management. Rapid advances in sensing and communication techniques make traffic speed detection easier than ever. However, due to sparse deployment of static sensors or low penetration of mobile sensors, speeds detected are incomplete and far from network-wide use. In addition, sensors are prone to error or missing data due to various kinds of reasons, speeds from these sensors can become highly noisy. These drawbacks call for effective techniques to recover credible estimates from the incomplete data. In this work, we first identify the problem as a spatiotemporal kriging problem and propose a unified graph embedded tensor (SGET) learning framework featuring both low-rankness and multi-dimensional correlations for network-wide traffic speed kriging under limited observations. To be specific, three types of speed correlation including temporal continuity, temporal periodicity, and spatial proximity are carefully chosen. We then design an efficient solution algorithm via several effective numeric techniques to scale up the proposed model to network-wide kriging. By performing experiments on two public million-level traffic speed datasets, we finally draw the conclusion and find our proposed SGET achieves the state-of-the-art kriging performance even under low observation rates, while at the same time saving more than half computing time compared with baseline methods. Some insights into spatiotemporal traffic data kriging at the network level are provided as well.

Keywords: Network-wide traffic estimation, traffic speed correlation, spatiotemporal kriging, low-rank tensor learning, graph tensor model, missing data

1. Introduction

Traffic speed is the central macroscopic quantity used to characterize the fluidity of the road network. Many applications in the transportation domain rely on the knowledge of traffic speed over the road network to support various dimensions of decision-making, such as real-time navigation, dynamic route planning, congestion management, pollution evaluation, and infrastructure optimization (Boriboonsomsin et al., 2012; Liebig et al., 2017; Liu et al., 2019; Han et al., 2020). With rapid advances in sensing and communication techniques, collecting traffic speed measurements becomes easier than ever: static sensors such as loop detectors are continuously logging vehicular speeds past a cross-section, while mobile sensors such as floating cars are chronicling speeds of their background traffic flow. In fluid mechanics' terminology, static sensors generate Eulerian measurements at fixed locations, while mobile sensors produce Lagrangian measurements following the flow as they move. To obtain a full picture of the network-wide traffic speed, either Eulerian measurements with dense sensor deployments or Lagrangian measurements with high vehicular penetration rates is desired, whereas in fact the reality is far from desirable.

One may see in reality that the static sensors often have a sparse coverage subject to high installation budget and maintenance costs and leave many road links undetected, thereby rendering low spatial resolution data that is hard to extend to the entire network. In the meanwhile, mobile sensors, which are mostly installed on commercial vehicle fleets like taxis, often result in a low penetration rate, which may render dubious speed estimation due to its biased representation of the population. In addition, sensors are prone to error or missing data due to various kinds of reasons such as equipment failure, communication outage, and out-of-service, speeds detected from these sensors can become highly noisy (Asif et al., 2016). These drawbacks combined imply that the sensing data is by no means ideal, and call for effective techniques to recover credible estimates from the incomplete data. Fortunately, traffic speeds bounded in the road network are highly correlated in both space and time, and therefore pose a rich degree of redundancy (or low-rankness in a matrix or tensor theory's term (Tan

^{*}Corresponding author. Address: Cao'an Road 4800, Shanghai 201804, China Email address: sunjian@tongji.edu.cn (Jian Sun)

et al., 2013)) that undetected or erroneous speeds of some road links are recoverable by virtue of the correlation. In other words, sparse sensors are able to achieve a "collaborative perception" of traffic speeds of the undetected road links, when their intrinsic multi-dimensional correlations are effectively exploited (see Fig. 1).

Recent years have witnessed a vast array of studies investigating the problem of estimating traffic state on undetected road links (Meng et al., 2017; Zhang et al., 2020; Wu et al., 2021a; Lei et al., 2022). This problem is often cast into spatiotemporal traffic kriging (Wu et al., 2021a) in the literature. Unlike the traffic forecasting problem that aims at predicting future state of a road link given its historical state, spatiotemporal traffic kriging attempts to estimate the traffic state of an undetected road link without any historical state of that link; it instead needs to utilize measurements of other detected road links to complete the "spatial prediction." Kriging is therefore regarded as a special missing data imputation problem. How to effectively utilize the correlation between undetected road links and other sparsely detected roads is the core research question of this paper. Upon close inspection, we identify three-fold specific challenges:

First, correlation between speeds of the detected road links and speeds of the undetected ones can be arbitrary unless reasonable prior assumptions are made. Low-rankness is a widely-adopted general prior in literature to reflect linear correlation of traffic data over space (Tan et al., 2013; Asif et al., 2016; Chen et al., 2021a). However, low-rankness is not applicable to our kriging problem in which data are fully missing in some locations, as in this case, we can fill different sets of values to the missing data without changing the rank and the missing values therefore remain undetermined under the low-rankness assumption. Conceptually, low-rankness is not sufficient when imputing a space-time matrix with entire row or column missing. Additional regularization terms should be carefully considered to complement the low-rankness assumption (Bahadori et al., 2014; Yokota et al., 2018; Yamamoto et al., 2022).

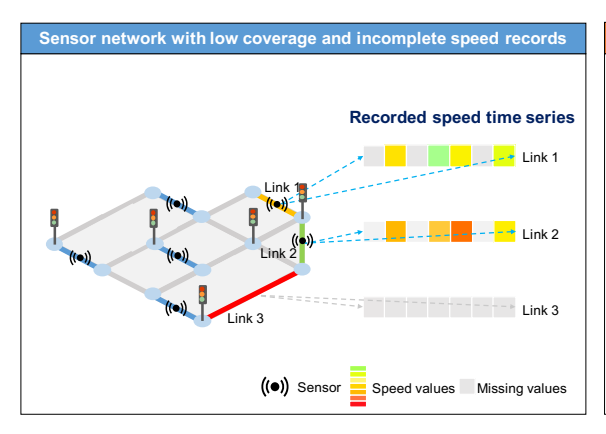
Second, in addition to general correlation assumptions, exploiting the semantic spatiotemporal correlation of speeds is an necessary add-on. Since speed manifests microscopic traffic that is time-varying, dynamic, periodic, and spatially interdependent, in the meanwhile, spatial correlation is bounded on a graph instead of on a 2D plane, spatial correlation should consider the graph features as well as traffic flow loaded on that graph(Li et al., 2017), exploiting spatio-temporal correlations is by no means trivial. Tailoring an effective kriging model to capture the multi-modal correlations of spatiotemporal traffic data is still an open question yet to be resolved.

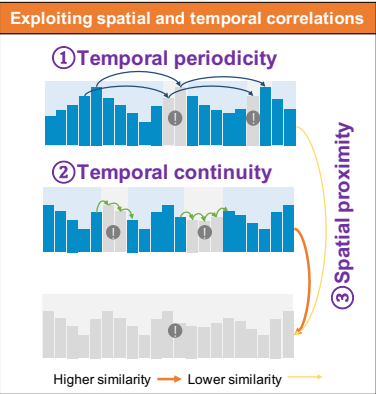
Third, scalability of the kriging approach onto the network level is desired as it allows exploiting correlation of a wider scope of speeds over space with added accuracy. Moreover, when new measurements are collected, a kriging model with fast parametric update is preferable for an online estimation. To this end, computational efficiency is the key. However, classical Gaussian process (GP) based kriging doesn't show scalability due to its computational complexity, while existing scalable tensor based imputation methods (Lu et al., 2019; Chen et al., 2021a) are mainly designed for general data imputation problem, and are not applicable to the kriging task. Although Bayesian Gaussian kriging methods achieve flexible hyper-parameter tuning for spatiotemporal kriging (Lei et al., 2022; Chen et al., 2022), its high consumption of time and memory in parametric learning of the Gaussian kernel inhibits itself from being scaled to the network level. Custom scalable solution algorithms need to be designed to maximize the kriging performance.

To tackle the challenges and realize a network-wide kriging of missing speed data for the undetected road links, we propose an integrated graph tensor-based framework to exploit the multi-modal spatiotemporal correlations of traffic speeds, where three kinds of carefully chosen speed correlation – *temporal continuity*, *temporal periodicity* and *spatial proximity* – are simultaneously captured. The framework contributes to the current literature in three aspects as follows:

- 1. We customize a new temporal graph Fourier transform (TGFT) to encode the temporal periodicity of speeds. The TGFT complements the low-rankness assumption and enables parallelization of the kringing processes by a series of daily matrix in graph spectral domain.
- 2. We embed spatial proximity and temporal continuity of speeds in space-time domain as an add-on to low-rankness and integrate them in a holistic graph tensor learning framework through a matrix-tensor conversion. Both global and local correlations can therefore be modeled simultaneously.
- 3. To scale up the kriging at network level, we propose a randomized singular value decomposition-based tensor singular value thresholding algorithm, and adopt conjugate gradient method to update matrix variables in an efficient manner. Both of the numeric techniques significantly reduce the computational burden while maintaining high accuracy.

The rest of this article is organized as follows. Section 2 reviews related works about spatiotemporal kriging. Section 3 introduces basic concepts about tensor operations in this work and defines the tensor-based kriging problem. In Section 4, we propose the graph tensor-based kriging model and a scalable solution algorithm. In Section 5, we perform numerical experiments of the proposed approach on two public data sets, which is followed by model comparison, ablation studies, and sensitivity analysis. Section 6 concludes this work and provides future directions.





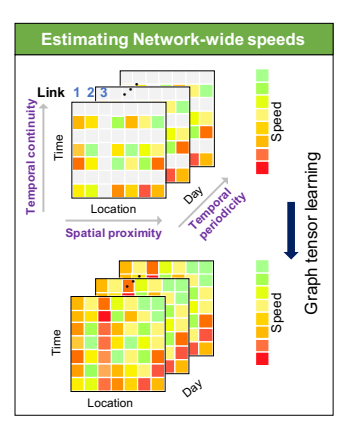


Figure 1: Illustration of spatiotemporal kriging problem. Take link 1, 2 and 3 as an example: link 1 and 2 record incomplete traffic speeds with missing time intervals, and link 3 are not equipped with a sensor so there is no historical record at all. The aim of spatiotemporal kriging is using the multi-dimensional spatial and temporal correlations (temporal continuity, temporal periodicity and spatial proximity) to infer the unmeasured locations (link 3) from the measured locations (link 1 and 2). In this figure, link 2 is physically closer to link 3 than link 1, so it is rational to assume link 2 and link 3 have stronger similarity.

2. Related work

Kriging is typically a regression problem for spatial modeling and interpolation of random fields based on covariance functions, which is a ubiquitous topic in geostatistics and usually associated with GP regression. Recently, kriging tasks have aroused great interests from different disciplines in machine learning community and many of these works can be viewed as special variants of kriging. In this section, we discuss kriging problems and summarize related solutions from a general perspective: spatial prediction with no historic data.

2.1. Graph regularized low-rank matrix and tensor completion based methods

In recommendation system community, graph regularized matrix completion/factorization models are commonly used for collaborative filtering tasks (Kalofolias et al., 2014; Rao et al., 2015; Strahl et al., 2020). The main purpose is to predict the unknown node values using side information about edges, which resembles the motivation of kriging. Kalofolias et al. (2014) first proposed a matrix completion model with graph Laplacian regularization. Rao et al. (2015) solved this problem in a scalable manner called graph regularized alternating least squares method, where conjugate gradient method was applied to update parameters. In the study of transportation, graph regularization is introduced either in space-time domain (Bahadori et al., 2014; Wang et al., 2018; Zhang et al., 2020; Yang et al., 2021), or graph spectral domain (Deng et al., 2021) to model spatial dependency. Among these works, Bahadori et al. (2014) proposed a tensor learning model for spatiotemporal co-kriging. The optimization problem was solved by greedy algorithm with orthogonal projections. Most of these works are developed for other data source and can not be directly transferred to our problem, as the unique characteristics of traffic speed should be taken into consideration.

2.2. Bayesian/probabilistic matrix factorization based method

Since kriging is a basic problem in GP modeling, some works combine GP priors with matrix factorization in a whole probabilistic framework to inference unknown data (Luttinen and Ilin, 2009; Zhou et al., 2012; Yang et al., 2018; Strahl et al., 2020). When graph Laplacian is specified as the kernel (covariance) function, this kind of model is equivalent to the graph regularized matrix factorization model. Most recently, Lei et al. (2022) proposed a Bayesian kernelized matrix factorization model for spatiotemporal traffic data imputation and kriging. Using a fully Bayesian treatment, this method can learn the hyper-parameters of graph kernels through resampling. One downside can not be overlooked is that the hyper-parameter sampling procedure is quite time-consuming. Therefore, there seems to be a trade-off between model scalability and flexibility.

2.3. Graph neural network based method

Graph convolution neural networks (GCN) has shown great potential for inductive modeling and achieved promising performances on kriging tasks (Appleby et al., 2020; Wu et al., 2021a,b; Liang et al., 2022). Appleby et al. (2020) first developed a kriging convolutional networks using K-nearest neighbor to reconstruct all the node values on a defined graph. Wu et al. (2021a) proposed an inductive GCN to model the spatial dependency and a random mask sample generation method was used for model training. However, both of these methods consider the sample over a specific observation time as individual or additional features, thus ignoring the temporal consistency. Liang et al. (2022) further improved the kriging performance of GCN by integrating an external attention mechanism and a temporal convolution network. Despite high accuracy has been achieved, training these elaborate GCN models is computationally very expensive and may require GPU hardware acceleration, which is prohibitive for large-scale problems.

2.4. Multi-way delay embedding (Hankelization) based methods

In the field of computer vision, kriging can be regarded as recovery of missing pixels along entire rows or columns of RGB images, i.e., a special image inpainting task (Yokota et al., 2018). Hankel matrix that bases on shift-invariant features of image is supposed to be a powerful tool for this issue. Yokota et al. (2018) proposed a Tucker tensor decomposition in multi-way delay-embedded (MDT) space method (aka., Hankelization) and extend the Hankel matrix to tensor. Yamamoto et al. (2022) further improved the scalability of Hankel tensor completion by using circulant MDT approximation. Although these pioneering works do not aim to solve spatiotemporal traffic kriging, the MDT based method has been applied to various transportation problems, such as traffic speed estimation from trajectories (Wang et al., 2021b), traffic data anomaly detection using RPCA (Wang et al., 2021a), and short-term traffic forecasting (Shi et al., 2020). In the context of spatiotemporal traffic data, there exists shift-invariant patterns in the time dimension, while this phenomenon is not distinctive in the space dimension. Without external spatial information, the MDT may produce erroneous kriging results.

3. Preliminaries and problem definitions

In this section, we first introduce some basic notation and preliminaries about tensor algebra. After that, we describe the spatiotemporal traffic speed kriging problem in the perspective of graph tensor learning framework.

3.1. Notation and basic concepts

Throughout this paper, we use the same notations as in (Kolda and Bader, 2009). Specifically, we adopt boldface capital letters to denote matrices, e.g., $\mathbf{M} \in \mathbb{R}^{M \times N}$, boldface lowercase letters, e.g., $\mathbf{a} \in \mathbb{R}^M$ to denote vectors, and scalars are denoted by lowercase letters, e.g., a. For a matrix \mathbf{M} , the i-th row and j-th column are abbreviated as \mathbf{M}^i , \mathbf{M}_j . A third-order tensor is denoted by calligraphic letter, e.g., $\mathcal{X} \in \mathbb{R}^{n_1 \times n_2 \times n_3}$, whose (i,j,k)-th entry is x_{ijk} , and we use the MATLAB notation $\mathcal{X}(i,:,:)$, $\mathcal{X}(:,i,:)$ and $\mathcal{X}(:,:,i)$ to denote the i-th horizontal, lateral and frontal slice, respectively. Specially, the frontal slice $\mathcal{X}(:,:,i)$ is denoted compactly as $\mathbf{X}^{(i)}$. A tubal fiber (mode-3 fiber) $\mathcal{X}(i,j,:)$ is obtained by fixing the first two indices and varying the third index. The inner product of two matrix is given by $\langle \mathbf{A}, \mathbf{B} \rangle = \mathrm{Tr}(\mathbf{A}^\mathsf{T}\mathbf{B})$, where $\mathrm{Tr}(\cdot)$ signifies the matrix trace. The inner product of two third-order tensors is defined by $\langle \mathcal{A}, \mathcal{B} \rangle = \sum_{i,j,k} a_{i,j,k} b_{i,j,k}$, and the corresponding tensor Frobenius norm is $\|\mathcal{A}\|_F = \sqrt{\langle \mathcal{A}, \mathcal{A} \rangle}$.

For matrices, we introduce the reshaping and vectorization operation for efficient matrix-vector product. If $\mathbf{X} \in \mathbb{R}^{M \times N}$, then the vectorization of \mathbf{X} denoted by $\text{vec}(\mathbf{X})$ is an NM-by-1 vector obtained by stacking the columns of \mathbf{X} :

$$vec(\mathbf{X}) = \begin{bmatrix} \mathbf{X}(:,1) \\ \vdots \\ \mathbf{X}(:,N) \end{bmatrix}. \tag{1}$$

Let $\mathbf{A} \in \mathbb{R}^{m \times n}$ and $m_1 n_1 = mn$, then the outcome of reshaping \mathbf{A} :

$$\mathbf{B} = \text{reshape}(\mathbf{A}, m_1, n_1) \tag{2}$$

is a m_1 -by- n_1 matrix defined by $vec(\mathbf{B}) = vec(\mathbf{A})$.

Graph Laplacian serves as a regularization term and has ubiquitous applications in geometric matrix factorization models (Kalofolias et al., 2014; Rao et al., 2015). Given an undirected and possibly weighted graph $\mathscr{G} = (\mathscr{N}, \mathscr{E}, \mathbf{W})$ with nodes \mathscr{N} and edges $\mathscr{E} \subseteq \mathscr{N} \times \mathscr{N}$ weighted with a non-negative weight matrix (adjacent matrix) \mathbf{W} , the graph Laplacian is calculated from the weight matrix:

$$\mathbf{Lap} = \mathbf{D} - \mathbf{W}, \mathbf{D} = \operatorname{Diag}(\sum_{i'} w_{ii'}). \tag{3}$$

Invertible linear transform, is proved to be a flexible tool for different real data formatted as tensors (Lu et al., 2019). Given an invertible linear transform, one can establish a transform induced tensor product (t-product) and tensor singular value decomposition (t-SVD) accordingly. Let $\mathbf{L} \in \mathbb{C}^{n_3 \times n_3}$ be an arbitrary invertible transform matrix (e.g., discrete Fourier transform (DFT), discrete cosine/sine transform (DCT/DST), unitary transform (UT) and graph Fourier transform (GFT)) that satisfies:

$$\mathbf{L}\mathbf{L}^{\mathsf{H}} = \mathbf{L}^{\mathsf{H}}\mathbf{L} = l\mathbf{I}_{n_0},\tag{4}$$

where l > 0 is a constant and H is the conjugate transposition, then given a third-order tensor $\mathcal{X} \in \mathbb{R}^{n_1 \times n_2 \times n_3}$, the transform matrix is applied on each tube fiber $\mathcal{X}(i, j, :)$ along the **third-dimension** of \mathcal{X} , i.e.,

$$\bar{\mathcal{X}}(i,j,:) = \mathbf{L}\mathcal{X}(i,j,:),\tag{5}$$

which is equivalent to:

$$\bar{\mathcal{X}} = \mathcal{L}(\mathcal{X}) = \mathcal{X} \times_3 \mathbf{L},\tag{6}$$

where we use $\mathcal{L}(\cdot)$ to denote the linear transform operator, $\bar{\mathcal{X}}$ is the transformed tensor, and \times_3 denotes the mode-3 product (Kolda and Bader, 2009). Similarly, the inverse transform is given by:

$$\mathcal{X} = \mathcal{L}^{-1}(\bar{\mathcal{X}}) = \bar{\mathcal{X}} \times_3 \mathbf{L}^{\mathsf{H}}.\tag{7}$$

To give an intuitive example, when we adopt the DFT, the transformed tensor can be obtained by performing DFT of \mathcal{X} along the third-dimension, i.e., $\bar{\mathcal{X}} = \mathrm{fft}(\mathcal{X}, [\], 3)$ by using the MATLAB command fft.

The mechanism of transformed tensor completion is that by imposing transform along certain dimension, the whole tensor completion problem can be divided into solving a series of small-scale matrix completion problems for each frontal slice $\bar{\mathcal{X}}^{(i)}$, and their solutions are then concatenated through inverse transform. This treatment reduces the computational cost of tensor completion and enable us to perform it on large-scale data set by computing in parallel.

Like the product of two matrices, the product of two tensors induced by linear transform can be defined analogously.

Definition 1. (t-product (Lu et al., 2019; Song et al., 2020)) Given any invertible transform \mathcal{L} , and $A \in \mathbb{R}^{n_1 \times n_2 \times n_3}$ and $\mathcal{B} \in \mathbb{R}^{n_1 \times n_2 \times n_3}$, then the transform based t-product denoted as $C = A *_{\mathcal{L}} \mathcal{B}$, is defined such that $\bar{\mathbf{C}}^{(i)} = \bar{\mathbf{A}}^{(i)} \bar{\mathbf{B}}^{(i)}$, for $i = 1, \ldots, n_3$.

Note that $\bar{\mathbf{C}}^{(i)} = \bar{\mathbf{A}}^{(i)}\bar{\mathbf{B}}^{(i)}$ can be denoted compactly using the block diagonal matrix. Def. 1 implies that the transform induced t-product can be performed by the matrix-matrix product in the transform domain. In the following sections, we will adopt this t-product to achieve some important tensor operations in the graph spectral domain.

3.2. Graph-regularized low-rank tensor learning for traffic speed kriging

Spatiotemporal traffic speed kriging can be treated as a special data imputation problem on a pre-specified graph so that we can model it through a tensor completion/learning method. Specifically, given an observation speed matrix $\mathbf{Z} \in \mathbb{R}^{(IK) \times J}$ whose rows correspond to IK uniformly distributed time points with I time intervals per day within K days, and columns correspond to sensors at J locations, the objective of spatiotemporal kriging in this paper can be described as learning the graph signals (node values) at unmeasured locations (entire columns) and missing time intervals (entire rows), given the observations and graph structure. This can be formulated as maximum of a posterior probability (MAP):

$$\hat{\mathbf{Z}} = \arg \max_{\mathbf{Z}} P(\mathbf{Z}|\mathbf{Z}_{\Omega}, \mathcal{G}_r, \mathcal{G}_c), \tag{8}$$

where $P(\cdot|\cdot)$ is the conditional probability function, Ω is the index where rows and columns are measured. \mathscr{G}_r and \mathscr{G}_c are prior information about rows and columns, i.e., temporal and spatial correlations in our case. From the perspective of tensor completion model, MAP is equivalent to the following form:

$$\min_{\mathcal{X}} \|\mathcal{X}\|_{\text{norm}} + \mathcal{R}_s(\mathcal{X}) + \mathcal{R}_t(\mathcal{X}),$$
s.t.
$$\begin{cases}
\mathbf{P} \odot \mathbf{Z} = \mathbf{P} \odot \mathbf{T}, \\
\mathcal{X} = \mathcal{T}(\mathbf{Z}),
\end{cases}$$
(9)

where $\|\mathcal{X}\|_{\text{norm}}$ is the tensor norm of \mathcal{X} to approximate the tensor rank, $\mathcal{R}_s(\cdot), \mathcal{R}_t(\cdot)$ are spatial and temporal consistency regularization, respectively. \mathbf{P} is an indicating matrix whose entry is 1 when this data point is observed and 0 otherwise. \mathbf{T} is the partially observed matrix, \odot is the Hadamard product. Note that $\mathcal{T}(\cdot): \mathbb{R}^{(IK)\times J} \to \mathbb{R}^{I\times J\times K}$ denotes a forward tensorization operator that converts the spatiotemporal matrix into a third-order tensor of shape (time of day × locations × days) by stacking the 'day' dimension (Chen et al., 2021b). Conversely, the inverse matricization operator is denoted by $\mathcal{T}^{-1}(\cdot)$.

The first term in Eq. (9) encourages the tensor norm (Kolda and Bader, 2009) to be small (or rank to be low) which serves as a global soft constraints. Low-rank (small-norm) pattern can capture inherent redundancy and linearity of traffic data. In this work, we establish a new temporal graph Fourier transform based tensor nuclear norm (t-TNN). Moreover, it is not hard to find that the unmeasured rows and columns of a time-space matrix is manifested as some missing 'slices' of a tensor. Purely low-rank model is incapable of dealing with such 'missing slices' of tensor, because it is agnostic to the positional information (Nie et al., 2022). Therefore, the other two terms are designed for encoding side information about rows and columns, which are in fact local hard constraints. Overall, Eq. (9) is a simultaneous structured model that encourages sparsity of $\mathcal X$ in the tensor singular value vector outer product space, and column-row wise sparsity of $\mathbf Z$ in the spatial and temporal Laplacian eigenspaces. The proposed method mainly features tensor norm minimization and spatial-temporal regularization, which favors a globally low-rank and locally smooth solution.

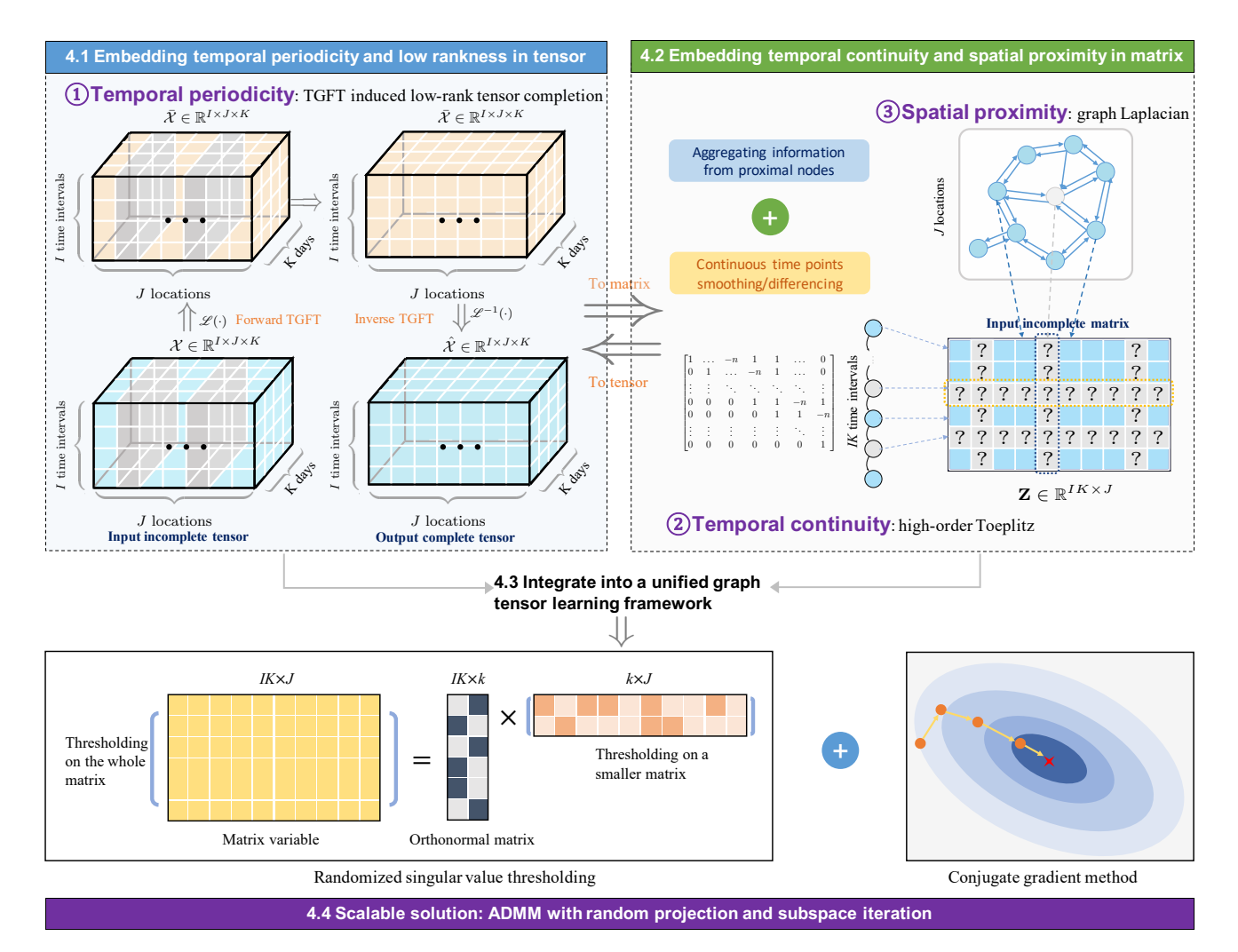


Figure 2: Illustration of proposed SGET framework. The whole method features three parts: embedding temporal periodicity and low rankness with temporal graph Fourier transform (in 4.1), modeling temporal continuity with high-order Toeplitz, and encoding spatial proximity with graph Laplacian (in 4.2). All these designs are integrated into a graph tensor learning model (in 4.3) and we obtain a scalable solution in 4.4.

4. Methodology

In this section, we first introduce a novel temporal graph Fourier transform (TGFT) and the corresponding linear transform-induced tensor nuclear norm. Since then, we establish the temporal and spatial regulations by high-order Toeplitz matrix and graph Laplacian, respectively. Finally, we formulate the tensor completion model for traffic speed kriging and solve it in a highly scalable manner using the alternating direction method of multipliers (ADMM) with some valuable numeric techniques, i.e., randomized tensor singular value thresholding (r-tSVT) and conjugate gradient (CG). The proposed model is referred to as Spatiotemporal Graph Embedded Tensor (SGET) learning. The proposed framework is shown in Fig. 2.

4.1. Embedding temporal periodicity and low rankness with temporal graph Fourier transform

As described in Section 3, invertible linear transform serves as an important role in scalable tensor completion methods. The most common transforms such as FFT, DCT, are adopted for image or video data (Lu et al., 2016, 2019). Nevertheless, how to determine a knowledge-based transform for traffic data is still worthy to be considered. In the existing literature of transportation, Chen et al. (2021a) used a data-driven unitary transform which is obtained by the SVD of day-mode unfolding; Deng et al. (2021) performed GFT along the 'location' dimension to extract the graph information. Recall that we arrange the data in a tensor of (time of day \times locations \times days) format, if the linear transform is performed on the 'days' mode, dealing with each daily subproblem of transformed tensor separately may ignore the temporal periodicity of traffic data.

To take advantage of prior knowledge about spatiotemporal traffic data, we establish a novel temporal graph Fourier transform (TGFT) based on classical GFT. GFT has been widely applied into the graph spectral analysis and the emerging graph neural networks to capture the non-Euclidean relationships on graphs (Kipf and Welling, 2016). The basic GFT is defined as:

Definition 2. (GFT (Shuman et al., 2013)) Given a graph signal $\mathbf{f} \in \mathbb{R}^{n_3}$ and the graph Laplacian Lap, the GFT of \mathbf{f} is

$$\bar{\mathbf{f}} = GFT(\mathbf{f}) = \mathbf{U}\mathbf{f},$$
 (10)

and the inverse operator is

$$f = iGFT(\bar{\mathbf{f}}) = \mathbf{U}^{\mathsf{H}}\bar{\mathbf{f}},$$
 (11)

where the transform matrix operator \mathbf{U} is obtained by the eigenvalue decomposition $\mathbf{Lap} = \mathbf{U} \Lambda \mathbf{U}^{\mathsf{H}}$.

To embed the multi-scale relationships of days and weeks, we establish the TGFT based on a temporal adjacent matrix that describes the correlations of days and weeks. The temporal adjacent matrix $\mathbf{A_t} \in \mathbb{R}^{K \times K}$ is given as:

 $a_{ij}^{t} = \begin{cases} 1 \text{ if } |i-j| = 1 \text{ or } |i-j| = 7, \\ 0 \text{ otherwise.} \end{cases}$ (12)

Intuitively, there is a direct connection if two days are consecutive or the same day of a week. Since A_t is nonnegative and symmetric, then the temporal graph Laplacian L_t is symmetric and semi-positive definite, which can be obtained from Eq. (3). Moreover, as L_t is real-valued, the resulted eigendecomposition $L_t = U_t \Lambda U_t^T$ is also real-valued. It is obvious that the TGFT operator U_t holds the property in Eq. (4) thus the forward and backward transform can be implemented for tensors using Eq. (6) and Eq. (7).

Each tubal fiber $\mathcal{X}(i,j,:)$ of the transformed tensor describes the graph signal at the i-th time interval in the j-th location within K days, and all fibers are controlled by a single temporal Laplacian. After performing TGFT, we are allowed to tackle the transformed matrix optimization subproblem for each day (which will be discussed in Section 4.4.1) and the 'day-to-day' and 'day-of-week' correlations (i.e., temporal periodicity) are encoded in the whole transformed tensor (see Fig. 2).

Compared with GFT performed on the 'location' mode in (Deng et al., 2021), when there exists a large number of sensors at network level ($J \gg I, K$), the proposed TGFT can split the original problem into much fewer (K) subproblems with well scalability, rather than J in original GFT.

Once we assign TGFT as the linear transform in Eq. (4), the corresponding transform based tensor nuclear norm (t-TNN) and tensor-tensor product (t-product) can be given as follows.

Definition 3. (t-TNN (Lu et al., 2019; Song et al., 2020)) The t-TNN of a tensor $A \in \mathbb{R}^{n_1 \times n_2 \times n_3}$ is the sum of the nuclear norms of all frontal slices of \bar{A} , i.e.,

$$\|\mathcal{A}\|_{t*} = \sum_{i=1}^{n_3} \|\bar{\mathbf{A}}^{(i)}\|_* = \|\widetilde{\mathbf{A}}\|_*, \tag{13}$$

where $\|\cdot\|_*$ denotes the matrix nuclear norm, $\widetilde{\mathbf{A}} \in \mathbb{R}^{n_1 n_3 \times n_2 n_3}$ is the block diagonal matrix of $\overline{\mathcal{A}}$ with its i-th block on the diagonal as the i-th frontal slice of $\overline{\mathcal{A}}$:

It has been proved that the above t-TNN is the convex envelope of the tensor tubal rank (Lu et al., 2019; Song et al., 2020). The motivation behind using t-TNN in this work is to preserve the low-rank property of traffic data tensor as well as to reduce the computational cost as much as possible. Traditionally, the tensor rank is approximated by the sum of nuclear norm or Schatten p-norm of all unfolding matrices (Chen et al., 2021b; Nie et al., 2022), and the SVD needs to be conducted on all unfolding matrices. Consider that we assume $n_2 \gg n_1 > n_3$ for large-scale problems, this yields time complexity of $\mathcal{O}(n_1^2n_2n_3 + n_1n_2n_3 \min\{n_2, n_1n_3\} + n_1n_2n_3^2)$ in total. While under the definition of t-TNN, SVD only needs to be computed on n_3 frontal slices of size $n_1 \times n_2$ and the time complexity reduces to $\mathcal{O}(n_1^2n_2n_3)$.

Induced by TGFT, we are allowed to perform t-TNN optimization in the domain of graph spectral, and obtain the output tensor in original space-time domain through inverse TGFT. This can be viewed as a feature augmentation by coordinate transformation, where a new subspace benefiting low-rankness is chosen.

4.2. Modeling spatial proximity and temporal continuity for local constraints

Performing tensor nuclear norm minimization (i.e., Eq. (13)) can solve the missing data imputation problem with element-like or fiber-like missing patterns (Nie et al., 2022). However, when there exists entire missing slices of a tensor, using pure low-rank assumption could be undesirable as the original tensor structure is not sensitive to the permutation of tensor fibers. Therefore, the key to model kriging as a tensor completion problem is to exploit side information as physic guidance. Formally, we construct temporal continuity and spatial proximity regularization by adopting high-order Toeplitz matrix and spatial graph Laplacian respectively.

In time dimension, we establish the 'time-of-day' relationship (i.e., temporal continuity) explicitly by extra regularization, because the 'day-to-day' and 'day-of-week' correlations are alreasdy embedded in the transformed tensor by TGFT. For traffic data imputation and forecasting problems, some elaborate time series models such as vector autoregressive (Yu et al., 2016; Chen et al., 2021b), long-short term memory neural network (Yang et al., 2021), quadratic variation (Chen et al., 2021a), are adopted to capture complex and long-term temporal dynamics. While at the same time, more computational burdens are brought to train such temporal models. Nevertheless, Wu et al. (2021b) found that the temporal receptive field (temporal relationship) only has marginal impacts on the kriging performance. Therefore, we utilize a simple Toeplitz matrix to consider the temporal continuity and keep the scalability of model at the same time. The first-order and n-th (n > 1) order Toeplitz matrices are defined as:

$$\mathbf{E_{1}} = \begin{bmatrix} 1 & -1 & 0 & \dots & 0 & 0 & 0 \\ 0 & 1 & -1 & \dots & 0 & 0 & 0 \\ \vdots & \vdots & \ddots & \ddots & \vdots & \vdots & \vdots \\ \vdots & \vdots & \vdots & \ddots & \ddots & \vdots & \vdots \\ 0 & 0 & 0 & 0 & 1 & -1 & 0 \\ 0 & 0 & 0 & 0 & 0 & 0 & 1 \end{bmatrix}_{I \times I}, \mathbf{E_{n}} = \begin{bmatrix} 1 & \dots & -n & 1 & 1 & \dots & 0 \\ 0 & 1 & \dots & -n & 1 & \dots & 0 \\ \vdots & \vdots & \ddots & \ddots & \ddots & \ddots & \vdots \\ 0 & 0 & 0 & 1 & 1 & -n & 1 \\ 0 & 0 & 0 & 1 & 1 & -n & 1 \\ 0 & 0 & 0 & 0 & 1 & 1 & -n \\ \vdots & \vdots & \vdots & \vdots & \vdots & \ddots & \vdots \\ 0 & 0 & 0 & 0 & 0 & 0 & 1 \end{bmatrix}_{I \times I}. \tag{14}$$

Note that the order n should be even. It can be found that $\mathbf{E_1}$ is an upper triangular matrix with the main diagonal given by ones and the first upper diagonal given by negative ones. Similarly, $\mathbf{E_n}$ is also an upper triangular matrix with the first $[1,\ldots,n/2]$ and $[n/2+1,\ldots,n+1]$ upper diagonals given by ones, and the (n/2+1)-th upper diagonal being -n. This matrix can be calculated and stored in advance according to the kriging time span.

Having said all of above, the temporal continuity regularization is given as following:

$$\mathscr{R}_t(\mathbf{Z}) = \|\mathbf{E_n}\mathbf{Z}\|_F^2. \tag{15}$$

The function of Toeplitz regularization is to make consecutive time points to be similar, and Eq. (15) is in fact the total differences of multivariate time series. The higher the order, the longer the temporal receptive field. Thus, we can adopt Toeplitz matrix with diverse orders to impose temporal smoothness on the 'time interval' dimension flexibly.

As for spatial dimension, spatial graph Laplacian is adopted to construct spatial dependency on a graph structure, which is a vital component of kriging models. As described in Eq. (3), we establish a graph Laplacian based on sensor physical graphs. Specifically, we assume that the spot speed recorded by a static detector (e.g., loop sensor) tends to be similar with the value of its neighbor sensors. Thus we treat all sensors as nodes $\mathcal{V} = \{v_1, \dots, v_n\}$ and the connectivity of them as edges with weights $\mathbf{A_s}$ representing similarities.

In this work, we calculate the weights matrix by Gaussian kernel function:

$$a_{ij}^s = \exp\left(-\left(\frac{\operatorname{dist}(v_i, v_j)}{\sigma}\right)^2\right),$$
 (16)

where $\operatorname{dist}(v_i, v_j)$ is the physical distance between sensor v_i and v_j , which can obtained from the travel distance or the coordinate position; σ is the standard deviation of the distance matrix.

By performing Eq. (3), the graph Laplacian of sensor graph is derived by $\mathbf{L_s} = \mathrm{Diag}(\sum_j a_{ij}^s) - \mathbf{A_s}$, and the spatial dependency regularization can be formulated as following:

$$\mathscr{R}_s(\mathbf{Z}) = \sum_{j,j'} a_{jj'}^s \|\mathbf{z}_j - \mathbf{z}_{j'}\|_2^2 = \text{Tr}(\mathbf{Z}\mathbf{L}_s\mathbf{Z}^\mathsf{T}).$$
(17)

The intuition behind Eq. (17) is to impose a column-wise difference and control the weighted sum. This operation can encode the local spatial dependency and impute the unknown node values by aggregating referable information from measured ones. Moreover, one can find that $\mathcal{R}_t(\mathbf{Z})$ also has similar form and can be viewed as a special case of graph Laplacian with weights being one. Both of them are operating on a non-euclidean space representing the relationship of sensors, rather than the space-time domain.

4.3. Low-rank tensor learning with spatiotemporal information embedding

Having introduced all the components of model above, we now integrate the low-rank optimization part with spatial and temporal regularization in a unified tensor learning framework, making Eq. (9) the following specific form:

$$\min_{\mathcal{X}} \|\mathcal{X}\|_{t*} + \frac{\lambda_1}{2} \operatorname{Tr}(\mathbf{Z} \mathbf{L_s} \mathbf{Z}^{\mathsf{T}}) + \frac{\lambda_2}{2} \|\mathbf{E_n} \mathbf{Z}\|_F^2
\text{s.t. } \mathbf{P} \odot \mathbf{Z} = \mathbf{P} \odot \mathbf{T}, \mathcal{X} = \mathscr{T}(\mathbf{Z}),$$
(18)

where λ_1 and λ_2 are model hyper-parameters to balance the scale of t-TNN and extra regularization, $\mathcal{X} \in \mathbb{R}^{I \times J \times K}$ or $\mathbf{Z} \in \mathbb{R}^{(IK) \times J}$ are the target variables.

Eq. (18) is a transductive semi-supervised learning model, which means that the model training and inference process are in the same stage. The motivation of using the tensorization operator $\mathcal T$ to connect tensor with matrix is that we can impose regularization on columns and rows of the spatiotemporal matrix directly, and utilize the t-TNN of tensor to achieve 'low-rank' in the graph spectral domain simultaneously, without pre-specified rank parameter as in (Kolda and Bader, 2009). Another important reason is that the optimization problem of typical tensor completion is usually coupled (Liu et al., 2013), and we can decouple it using the connection between tensor and matrix with no need for introducing extra auxiliary variables.

4.4. Scalable solution with ADMM

It can be seen that after incorporating the spatial and temporal regularizers the model updating process confronts with more computational overhead, because both the Toeplitz and graph Laplacian are item-by-item smoothing operators and more computations are introduced. A traditional choice for solving tensor completion problem is the alternating direction method of multipliers (ADMM) method (Liu et al., 2013). ADMM is an iterative algorithm very suitable for numerous convex problems and the basic idea is to update each independent variable in a proper order for each epoch until the convergence.

We first give the basic formulation of ADMM. The corresponding augmented Lagrange function of Eq. (18) is defined as:

$$\mathscr{F}_{\mu}(\mathcal{X}, \mathbf{Z}, \mathcal{Y}) = \|\mathcal{X}\|_{t*} + \frac{\lambda_{1}}{2} \operatorname{Tr}(\mathbf{Z} \mathbf{L}_{s} \mathbf{Z}^{\mathsf{T}}) + \frac{\lambda_{2}}{2} \|\mathbf{E}_{n} \mathbf{Z}\|_{F}^{2} + \langle \mathcal{Y}, \mathcal{X} - \mathscr{T}(\mathbf{Z}) \rangle + \frac{\mu}{2} \|\mathcal{X} - \mathscr{T}(\mathbf{Z})\|_{F}^{2},$$
(19)

where \mathcal{Y} is the Lagrange dual variable tensor, μ is the penalty parameter of equality constraint as well as the learning rate. Note that we do not incorporate the constraint $\mathbf{P} \odot \mathbf{Z} = \mathbf{P} \odot \mathbf{T}$ into \mathscr{F}_{μ} as we directly use this equality to transfer observations. Then, the ADMM alternately minimizes each of the target variable and dual variable until convergence. The iterative scheme of ADMM leads to the following updating rules:

$$\begin{cases}
\mathcal{X}^{j+1} = \arg\min_{\mathcal{X}} \mathscr{F}_{\mu}(\mathcal{X}, \mathbf{Z}^{j}, \mathcal{Y}^{j}), \\
\mathbf{Z}^{j+1} = \arg\min_{\mathbf{Z}} \mathscr{F}_{\mu}(\mathcal{X}^{j+1}, \mathbf{Z}, \mathcal{Y}^{j}), \\
\mathcal{Y}^{j+1} = \mathcal{Y}^{j} + \mu \left(\mathcal{X}^{j+1} - \mathscr{T}(\mathbf{Z}^{j+1})\right).
\end{cases} (20)$$

For j-th iteration, we need to compute the optimal solution to each subproblem so that the ADMM guarantees the ideal solution. However, the overall computational efficiency is determined by the complexity of each subproblem and declines dramatically with the increase of problem scale.

As discussed in section 1, there exists a wealth of spatial correlations to be mined on the entire road network and integrating network-wide of data could contain more comprehensive relationships. In order to make the proposed model in Eq. (18) scalable to large network, we reformulate the ADMM scheme by improving the computation of each subproblem. Technically, we find the bottleneck (the highest time complexity) of each updating rule and accelerate it with numeric approximation methods: refining the solutions to $\mathcal X$ and $\mathbf Z$ subproblems using random projection and subspace iterative techniques separately. As can be found below, these useful designs make the model scalable to large-scale problems while keep high accuracy.

4.4.1. Solving X subproblem with random projection

To update \mathcal{X} variable, we first arrange the first line in Eq. (20) in the standard form of t-TNN minimization:

$$\mathcal{X}^{j+1} = \arg\min_{\mathcal{X}} \mathscr{F}_{\mu}(\mathcal{X}, \mathbf{Z}^{j}, \mathcal{Y}^{j}),$$

$$= \arg\min_{\mathcal{X}} \|\mathcal{X}\|_{t_{*}} + \langle \mathcal{Y}^{j}, \mathcal{X} - \mathscr{T}(\mathbf{Z}^{j}) \rangle + \frac{\mu}{2} \|\mathcal{X} - \mathscr{T}(\mathbf{Z}^{j})\|_{F}^{2},$$

$$= \arg\min_{\mathcal{X}} \|\mathcal{X}\|_{t_{*}} + \frac{\mu}{2} \|\mathcal{X} - (\mathscr{T}(\mathbf{Z}^{j}) - \mathcal{Y}^{j}/\mu)\|_{F}^{2}.$$
(21)

Under the definition of t-TNN, a general choice for solving Eq. (21) is to resort to a proximity operator called tensor singular value thresholding (t-SVT). We give the result in Lemma 1 as follows.

Lemma 1. (t-SVT (Lu et al., 2019)) For any tensor $\mathcal{M} \in \mathbb{R}^{n_1 \times n_2 \times n_3}$, let \mathcal{L} be any invertible linear transform and the tensor singular value decomposition (t-SVD) is given by $\mathcal{M} = \mathcal{U} *_{\mathscr{L}} \mathcal{S} *_{\mathscr{L}} \mathcal{V}^\mathsf{T}$, then the optimal solution to the following problem

$$\min_{\mathcal{X}} \|\mathcal{X}\|_{t*} + \frac{\mu}{2} \|\mathcal{X} - \mathcal{M}\|_F^2,$$

is given by the t-SVT: $\mathscr{D}_{1/\mu}(\mathcal{M}) = \mathcal{U} *_{\mathscr{L}} \mathcal{S}_{1/\mu} *_{\mathscr{L}} \mathcal{V}^{\mathsf{T}}, \mathcal{S}_{1/\mu} = \mathscr{L}^{-1}([\mathscr{L}(\mathcal{S}) - \frac{1}{\mu}]_{+}), where <math>[t]_{+} = \max(t, 0)$.

The variables in Lemma 1 are all in the form of tensor and this operator simply performs the soft-thresholding rule to $\mathcal{L}(\mathcal{S})$. Practically, since the t-SVD can be computed by performing matrix SVD in the transformed domain (graph spectral domain in this work), the t-SVT described above can also be calculated in an easy-to-understand fashion based on the definition of t-product (see Def. 1). Algorithm 1 summarizes the procedure to obtain $\mathcal{D}_{1/\mu}(\mathcal{M})$.

Algorithm 1: computation of t-SVT based on t-product $*_{\mathscr{L}}$

```
Input: \mathcal{M} \in \mathbb{R}^{n_1 \times n_2 \times n_3}, invertible transform \mathscr{L}, thresholding parameter 1/\mu. Output: \mathscr{D}_{1/\mu}(\mathcal{M}).

1 \bar{\mathcal{M}} \leftarrow \mathscr{L}(\mathcal{M});

2 compute each frontal slice of \bar{\mathcal{U}}, \bar{\mathcal{S}}, \bar{\mathcal{V}} from the slices of \bar{\mathcal{M}} by:

3 for i=1 to n_3 do

4 \left[\bar{\mathbf{U}}^{(i)}, \bar{\mathbf{S}}^{(i)}, \bar{\mathbf{V}}^{(i)}\right] \leftarrow \operatorname{svd}(\bar{\mathbf{M}}^{(i)});

5 \left[\bar{\mathbf{S}}_{1/\mu}^{(i)} \leftarrow [\bar{\mathbf{S}}^{(i)} - 1/\mu]_+;

6 \left[\bar{\mathbf{M}}_{1/\mu}^{(i)} \leftarrow \bar{\mathbf{U}}^{(i)} \bar{\mathbf{S}}_{1/\mu}^{(i)} \bar{\mathbf{V}}^{(i)\mathsf{T}};

7 concatenate \bar{\mathbf{M}}_{1/\mu}^{(i)} along the third dimension to form \bar{\mathcal{M}}_{1/\mu};

8 \mathscr{D}_{1/\mu}(\mathcal{M}) \leftarrow \mathscr{L}^{-1}(\bar{\mathcal{M}}_{1/\mu}).
```

From Lemma 1 one can see that the \mathcal{X} subproblem boils down to solve a series of matrix SVT problems on daily slices along the third axis in the transformed domain and the temporal periodicity are preserved in the TGFT tensor. This is a significant advantage of t-TNN that makes it possible to be extended to large data sets. Moreover, as daily matrices are independent on each other, the computation can be conducted in a highly-parallel way.

Despite the t-TNN itself has reduced the computation cost to some extent, there is still space for improvement. The main bottleneck of Algorithm 1 is to compute the SVD of certain $n_1 \times n_2$ matrices and the per-iteration cost is $\mathcal{O}(n_1^2n_2n_3)$ as discussed in section 4.1. However, tensors with sensor numbers n_2 much larger than time intervals n_1 could suffer from high computational cost at each iteration. In fact, from the calculation procedure of SVT we can observe that exact and complete SVD calculation is unnecessary for thresholding operation, because only a few singular values larger than the threshold value can have an effect. To this end, we expect to reduce the computation burden by finding an approximation of partial SVD.

A desired choice is using the random projection method to accelerate the SVD, i.e., randomized SVD (rSVD) (Halko et al., 2011). The core idea of rSVD is using a random projection matrix to help identify the subspace that dominates the pattern of matrix. Then, a rank-*k* approximation of the original matrix can be obtained which further leads to the approximate SVD. In general, a Gaussian i.i.d matrix can be specified as the random projection, and the subspace's orthonormal basis can be computed by the QR decomposition (Golub and Van Loan, 2013). For more details about rSVD please refer to (Halko et al., 2011).

In light of this view, we can speed up the matrix SVT calculation by the following lemma, then we adapt it for t-SVT by the property of t-product:

Lemma 2. Let $\mathbf{A} = \mathbf{Q}\mathbf{B} \in \mathbb{R}^{m \times n}$, where $\mathbf{Q} \in \mathbb{R}^{m \times k}$ is partially orthonormal, then we have:

$$\mathscr{S}_{\tau}(\mathbf{A}) = \mathbf{Q}\mathscr{S}_{\tau}(\mathbf{B}),\tag{22}$$

where $\mathscr{S}_{\tau}(\cdot)$ denotes the matrix SVT operator, k is the rank of **A**.

Based on Lemma 2, we could avoid expensive computational burden by instead performing SVT on a smaller matrix $\mathbf{B} \in \mathbb{R}^{k \times n}$. If the orthonormal matrix \mathbf{Q} is available and suppose $m \geq n$, the complexity for SVD becomes $\mathcal{O}(nk^2)$, which is much cheaper than the original SVD.

To perform Lemma 2, there are two key points to carefully consider. One major challenge is how to get an appropriate \mathbf{Q} . Fortunately, the orthonormal basis can be computed from the procedure of rSVD using QR decomposition. Another task is to estimate the target rank k at each iteration of ADMM. An empirical observation is that during the training process of tensor completion, the rank increases over iterations since the missing values are filled gradually. By exploiting this prior, a simple but effective way is to set a small value at first and increase it gradually with iteration until the upper bound. Another insightful consideration of r-tSVT is that setting a small rank k in each epoch encourages the low-rank characteristics of the solution. As the threshold value $1/\mu$ decreases over iterations (to benefit convergence), a lower rank solution could improve the estimation accuracy in practice.

The whole process to get $\mathscr{D}_{1/\mu}(\widetilde{\mathcal{A}})$ is summarized in Algorithm 2. Since the above lemma is based on matrix

Algorithm 2: fast randomized t-SVT based on rSVD

```
Input: A \in \mathbb{R}^{n_1 \times n_2 \times n_3}, rank parameter k < \min\{n_1, n_2\}, power parameter p, oversampling parameter s,
                    transform \mathcal{L}, thresholding parameter 1/\mu.
     Output: Low rank approximation \mathcal{D}_{1/\mu}(\mathcal{A}) of \mathcal{D}_{1/\mu}(\mathcal{A}).
 1 \bar{\mathcal{A}} \leftarrow \mathcal{L}(\mathcal{A});
 2 sample a Gaussian random matrix: \Omega \leftarrow \text{randn}(n_1, k+s);
 for i = 1 to n_3 do
             \bar{\mathbf{G}} \leftarrow \bar{\mathbf{A}}^{(i)\mathsf{T}}\mathbf{\Omega};
 4
            conduct power iteration by:
  5
 6
            for j = 1 to p do
              \bar{\mathbf{G}} \leftarrow \bar{\mathbf{A}}^{(i)\mathsf{T}}\bar{\mathbf{A}}^{(i)}\bar{\mathbf{G}};
  7
            compute a reduced QR decomposition: \bar{\mathbf{Q}}^{(i)} \leftarrow \mathrm{QR}(\bar{\mathbf{G}});
 8
            \mathbf{\bar{B}}^{(i)} \leftarrow \mathbf{\bar{Q}}^{(i)\mathsf{T}}\mathbf{\bar{A}}^{(i)\mathsf{T}};
10 concatenate \bar{\mathbf{B}}^{(i)} and \bar{\mathbf{Q}}^{(i)} along the third dimension to form \bar{\mathcal{B}}, \bar{\mathcal{Q}} respectively;
11 compute the t-SVT of \bar{\mathcal{B}} using line 2-7 in Algorithm 1 to obtain \bar{\mathcal{B}}_{1/\mu};
12 \bar{\mathcal{A}}_{1/\mu} \leftarrow \bar{\mathcal{Q}} *_{\mathscr{L}} \bar{\mathcal{B}}_{1/\mu};
13 \mathscr{D}_{1/\mu}(\widetilde{\mathcal{A}}) \leftarrow \mathscr{L}^{-1}(\bar{\mathcal{A}}_{1/\mu}).
```

There are some expositions about Algorithm 2. In our case $n_1(I) < n_2(J)$, we first transpose each slice matrix $\bar{\mathbf{A}}^{(i)}$ from $n_1 \times n_2$ to $n_2 \times n_1$ such that the resulted small matrix $\bar{\mathbf{B}}^{(i)} \in \mathbb{R}^{k \times n_1}$ requires minimal computation for SVD. Moreover, a useful technique called power iteration is applied in line 5-7 in Algorithm 2 to improve the estimation accuracy of \mathbf{Q} and Halko et al. (2011) also found that in practice p=1 or 2 usually suffices.

Finally, by adopting Algorithm 2, the optimal solution to update \mathcal{X} in Eq. (21) is:

$$\mathcal{X}^{j+1} = \mathcal{D}_{1/\mu} \left(\mathcal{T}(\mathbf{Z}^j) - \mathcal{Y}^j/\mu \right). \tag{23}$$

4.4.2. Solving Z subproblem with conjugate gradient

The second term in Eq. (20) is the optimization of spatial proximity and temporal continuity regularization that closely related to kriging tasks. After introducing the (inverse) tensorization operator $\mathbf{Z} = \mathcal{T}^{-1}(\mathcal{X})$, we can update \mathbf{Z} in the form of matrix easily:

$$\mathbf{Z}^{j+1} = \arg\min_{\mathbf{Z}} \mathscr{F}_{\mu}(\mathcal{X}^{j+1}, \mathbf{Z}, \mathcal{Y}^{j}),$$

$$= \arg\min_{\mathbf{Z}} \frac{\lambda_{1}}{2} \operatorname{Tr}(\mathbf{Z} \mathbf{L}_{\mathbf{s}} \mathbf{Z}^{\mathsf{T}}) + \frac{\lambda_{2}}{2} \|\mathbf{E}_{\mathbf{n}} \mathbf{Z}\|_{F}^{2} + \langle \mathcal{Y}^{j}, \mathcal{X}^{j+1} - \mathscr{T}(\mathbf{Z}) \rangle + \frac{\mu}{2} \|\mathcal{X}^{j+1} - \mathscr{T}(\mathbf{Z})\|_{F}^{2},$$

$$= \arg\min_{\mathbf{Z}} \underbrace{\frac{\lambda_{1}}{2} \operatorname{Tr}(\mathbf{Z} \mathbf{L}_{\mathbf{s}} \mathbf{Z}^{\mathsf{T}}) + \frac{\lambda_{2}}{2} \|\mathbf{E}_{\mathbf{n}} \mathbf{Z}\|_{F}^{2} + \frac{\mu}{2} \|\mathbf{Z} - \mathscr{T}^{-1}(\mathcal{X}^{j+1} + \mathcal{Y}^{j}/\mu)\|_{F}^{2}}.$$

$$\mathscr{H}(\mathbf{Z})$$
(24)

Set the gradient of $\mathcal{H}(\mathbf{Z})$ to zero, we can have the least square solution:

$$\lambda_1 \mathbf{Z} \mathbf{L_s} + \lambda_2 \mathbf{E_n}^\mathsf{T} \mathbf{E_n} \mathbf{Z} + \mu \mathbf{Z} = \mu \mathcal{T}^{-1} (\mathcal{X}^{j+1} + \mathcal{Y}^j / \mu). \tag{25}$$

Eq. (25) is a standard Sylvester matrix equation in the form of $\mathbf{AX} + \mathbf{XB} = \mathbf{C}$. Typically, a direct manner to solve this system is vectorizing it into a standard linear equations, as shown in Eq. (26).

$$(\lambda_1 \mathbf{L_s} \otimes \mathbf{I}_{IK} + \lambda_2 \mathbf{I}_J \otimes \mathbf{E_n}^\mathsf{T} \mathbf{E_n} + \mu \mathbf{I}_{IJK}) \operatorname{vec}(\mathbf{Z}) = \mu \operatorname{vec}(\mathscr{T}^{-1}(\mathcal{X}^{j+1} + \mathcal{Y}^j/\mu)), \tag{26}$$

where \otimes is the Kronecker product, $\text{vec}(\cdot)$ denotes the vectorization operator, and \mathbf{I}_n denotes an identity matrix of size $n \times n$. This conversion holds due to the fact that $\text{vec}(\mathbf{A}\mathbf{X}\mathbf{B}) = (\mathbf{B}^\mathsf{T} \otimes \mathbf{A}) \text{vec}(\mathbf{X})$.

However, the computational complexity of this vectorized solution is $\mathcal{O}(I^3J^3K^3)$, which is both computationally expensive and memory-consuming for large-scale problems. An alternative solution for Sylvester system is using Bartels-Stewart method (Golub and Van Loan, 2013). Although the cost can be reduced to $\mathcal{O}(I^3K^3+J^3)$, it is still prohibitive in practice. Note that in our case **A** and **B** are highly structured, i.e., symmetric and positive definite, so that the matrix vector multiplies involving them can be efficient. Taking this into account, subspace iterative methods could potentially perform better for fixing this problem.

Conjugate gradient (CG) is a representative Krylov subspace iteration method and has been verified to be an efficient and stable manner in recent works (Kalofolias et al., 2014; Rao et al., 2015). One distinct advantage of CG is that it is nonparametric and requires only a small number of iterations to solve the structured linear system with desired accuracy. By using the vectorization operation in Eq. (26), we apply CG to such a symmetric

positive definite system to approximate its numeric solution. Details about CG is omitted for simplicity and we present the procedure for solving \mathbf{Z} variable in Algorithm 3.

Algorithm 3: Conjugate gradient for Z-subproblem

```
Input: \mathbf{Z} \in \mathbb{R}^{(IK) \times J}, \mathcal{X}, \mathcal{Y}, \mu, \mathbf{L_s}, \mathbf{E_n}, \lambda_1, \lambda_2, maximum iterations t. Output: Estimated variable \hat{\mathbf{Z}}.

1 \mathcal{V}(\mathbf{Z}) \leftarrow (\lambda_1 \mathbf{L_s} \otimes \mathbf{I}_{IK} + \lambda_2 \mathbf{I}_J \otimes \mathbf{E_n}^\mathsf{T} \mathbf{E_n} + \mu \mathbf{I}_{IJK}) \operatorname{vec}(\mathbf{Z});

2 \mathbf{r_0} \leftarrow \mu \operatorname{vec}(\mathcal{T}^{-1}(\mathcal{X}^{j+1} + \mathcal{Y}^{j}/\mu)) - \mathcal{V}(\mathbf{Z});

3 \mathbf{q_0} \leftarrow \mathbf{r_0};

4 \mathbf{for} \ i = 1 \ \mathbf{to} \ t \ \mathbf{do}

5 \mathbf{Q}_i \leftarrow \operatorname{reshape}(\mathbf{q}_i);

6 \alpha_i \leftarrow \mathbf{r}_i^\mathsf{T} \mathbf{r}_i / (\mathbf{q}_i^\mathsf{T} \mathcal{V}(\mathbf{Q}_i));

7 \mathbf{z}_{i+1} \leftarrow \mathbf{z}_i + \alpha_i \mathbf{q}_i;

8 \mathbf{r}_{i+1} \leftarrow \mathbf{r}_i - \alpha_i \mathcal{V}(\mathbf{Q}_i);

9 \beta_i \leftarrow \frac{\mathbf{r}_{i+1}^\mathsf{T} \mathbf{r}_{i+1}^*}{\mathbf{r}_i^\mathsf{T} \mathbf{r}_i};

10 \mathbf{q}_{i+1} \leftarrow \mathbf{r}_{i+1} + \beta_i \mathbf{q}_i;

11 \hat{\mathbf{Z}} \leftarrow \operatorname{reshape}(\mathbf{z}_t).
```

In Algorithm 3, each iteration only involves one single matrix-vector product, several inner products and scalar operations. This makes it highly scalable to large problems and we can incorporate it in the ADMM framework.

The main cost of Algorithm 3 is the matrix-vector product to calculate $\mathcal{V}(\mathbf{Q}_i)$ and the time complexity is $\mathcal{O}(I^2J^2K^2)$ for each inner CG iteration. What is noteworthy is that this cost can be further reduced if we first compute the matrix-matrix products in $\lambda_1\mathbf{Q}_i\mathbf{L}_s + (\lambda_2\mathbf{E_n}^\mathsf{T}\mathbf{E_n} + \mu\mathbf{I})\mathbf{Q}_i$ and then obtain $\mathcal{V}(\mathbf{Q}_i)$ using reshape(·) directly. And the complexity is essentially $\mathcal{O}(IJK(IK+J))$ in this case, which is substantially reduced compared to $\mathcal{O}(I^3J^3K^3)$ required by the vectorized solution.

4.4.3. Solution algorithm

Having solved each ADMM subproblem, the proposed SGET algorithm is finally summarized in Algorithm 4. In this implementation, the updating order follows $\{\mathcal{X}^j\Rightarrow\mathbf{Z}^j\Rightarrow\mathcal{Y}^j\}$ and the estimated data values can be returned either in matrix $\hat{\mathbf{Z}}$ or in tensor $\hat{\mathcal{X}}$. In line 8, we increase the penalty parameter as well as the learning rate μ to promote the convergence of ADMM, and also increase the target rank k for Algorithm 2. As we solve both of the two subproblems in a highly scalable routine, this algorithm is efficient for large-scale kriging tasks. Moreover, two most important hyper-parameters in Algorithm 4 are the regularization parameters λ_1, λ_2 . These coefficients function as a balance between t-TNN minimization and local consistency penalty, and we will discuss the impacts of them in Section 5.3.3.

Algorithm 4: Spatiotemporal graph embedded low-rank tensor learning for kriging

Input: Measured speed matrix \mathbf{T} , indicating matrix \mathbf{P} , linear transform \mathscr{L} , learning rate μ , initial rank parameter k, regularization terms and coefficients $\mathbf{L_s}$, $\mathbf{E_n}$, λ_1 , λ_2 , convergence condition ϵ .

```
Output: Estimated full matrix \hat{\mathbf{Z}}.
```

```
1 Initialize \mathcal{Y}^0 as zeros, and set \mathbf{P} \odot \mathbf{Z}^0 \leftarrow \mathbf{P} \odot \mathbf{T}, j \leftarrow 0;
    while not converged do
          Update \mathcal{X}^{j+1} by Eq. (23) and Algorithm 1, 2;
3
          Update \mathbf{Z}^{j+1} by Algorithm 3;
4
          Transmit the observations by setting P \odot \mathbf{Z}^{j+1} \leftarrow P \odot \mathbf{T};
          Update \mathcal{Y}^{j+1} by \mathcal{Y}^{j+1} \leftarrow \mathcal{Y}^j + \mu \left( \mathcal{X}^{j+1} - \mathcal{T}(\mathbf{Z}^{j+1}) \right);
          e^{j+1} \leftarrow \|\mathbf{Z}^{j+1} - \mathbf{Z}^j\|_F / \|\mathbf{Z}^j\|_F;
7
          Increase the learning rate \mu and rank parameter k with a fixed step;
8
          if e^{j+1} < \epsilon then
            Converge.
10
         j \leftarrow j + 1;
11
```

4.5. Overall computational complexity analysis

The computational complexity of each solving step is introduced separately and we give a brief summary and discussion here. Overall, the main cost of Algorithm 4 is t-SVT in \mathcal{X} -subproblem and CG in **Z**-subproblem. The step-by-step computational complexity of Algorithm 2 and 3 is summarized in Tab. 1 and Tab. 2, respectively.

Since lines 4-11 in Tab. 1 are conducted for each daily slice, their complexity become *K* times. As we can see, the main bottleneck of SGET is the matrix-vector product in CG iteration. But this implementation is efficient enough for large-scale applications.

Table 1: Time complexity analysis for Algorithm 2.

Line No.	Specific operation	Complex	ity
4	$ar{\mathbf{G}} \leftarrow ar{\mathbf{A}}^{(i)T}\mathbf{\Omega}$	$\mathcal{O}(kIJ)$	<u> </u>
7	$ar{\mathbf{G}} \leftarrow ar{\mathbf{A}}^{(i)T} ar{\mathbf{A}}^{(i)} ar{\mathbf{G}}$	$\mathcal{O}(kIJ)$	-
8	$\bar{\mathbf{Q}}^{(i)} \leftarrow \mathrm{QR}(\bar{\mathbf{G}})$	$\mathcal{O}(Jk^2)$	$\times K$
9	$\bar{\mathbf{B}}^{(i)} \leftarrow \bar{\mathbf{Q}}^{(i)T}\bar{\mathbf{A}}^{(i)T}$	$\mathcal{O}(kIJ)$	1
11	$\operatorname{svd}(\bar{\mathbf{B}}^{(i)})$	$\mathcal{O}(Ik^2)$)
12	$\bar{\mathcal{A}}_{1/\mu} \leftarrow \bar{\mathcal{Q}} *_{\mathscr{L}} \bar{\mathcal{B}}_{1/\mu}$	$\mathcal{O}(kIJK)$	

Table 2: Time complexity analysis for Algorithm 3.

Line No.	Specific operation	Complexity
1	Compute $\mathscr{V}(\mathbf{Z})$	$\mathcal{O}\left(IJK(J+IK)\right)$
2	Compute \mathbf{r}_0	$\mathcal{O}(IJK)$
6	$\alpha_i \leftarrow \mathbf{r}_i^T \mathbf{r}_i / (\mathbf{q}_i^T \mathscr{V}(\mathbf{Q}_i))$	$\mathcal{O}\left(IJK(J+IK)\right)$
7,8,10	Compute \mathbf{z}_{i+1} , \mathbf{r}_{i+1} , \mathbf{q}_{i+1}	$\mathcal{O}(IJK)$
11	$\beta_i \leftarrow \mathbf{r}_{i+1}^T \mathbf{r}_{i+1} / (\mathbf{r}_i^T \mathbf{r}_i)$	$\mathcal{O}(IJK)$

5. Case study

In this section, we conduct experiments to evaluate the kriging performance of the proposed SGET model on two real-world and network-wide traffic speed datasets under different settings. First we briefly describe the datasets and introduce some state-of-the-art kriging baseline models. Apart from model comparison, we also conduct various ablation studies and sensitivity studies for algorithmic analysis. All the experiments are carried out on a Windows 10 platform with Intel(R) Core(TM) i7-12700KF 3.60GHz CPU (12 cores in total) and 32 GB RAM. The NumPy implementation is shared in our GitHub repository: https://github.com/tongnie/tensor4kriging.

5.1. Data preparation and experiment setup

5.1.1. Spatiotemporal traffic speed datasets

As we aim to evaluate kriging performances on large data, two publicly available large-scale traffic speed datasets: PeMS-4W freeway speed data (Chen et al., 2021a) and Portland highway speed data are used for benckmark experiments. These datasets are briefly summarized as follows:

- PeMS-4W freeway loop speed data¹: Large-scale traffic speed data collected from 11160 loop sensors installed on the freeway in California. The speed records include the first 4 weeks in 2018 with a 5-min resolution and it can be organized in a spatiotemporal matrix of shape (8064×11160) or a tensor of shape $(288 \times 11160 \times 28)$. This data set also provides a travel distance based adjacent matrix. This data contains about 90 million observations.
- Portland highway loop speed data²: The Portland database provides 20-second granularity loop detector records from freeways in the Portland-Vancouver metropolitan region. We collect traffic speed data from 1057 loop sensors with a 15-minute resolution over 3 months (from January 1 to March 31, 2021). The data size is (8640×1057) in matrix or $(96 \times 1057 \times 90)$ in tensor. This data provides the location information of all sensors. This data contains about 10 million observations.

The input data is arranged in a third-order tensor of (time of day \times locations \times days) or a matrix of (time points \times locations). One can find that the 'location' dimension is much larger than the 'time of day' dimension for both of the two datasets. Different from other large datasets used for traffic prediction studies, which usually feature a large 'days' dimension, the two data with pretty large 'locations' dimension are more suitable for testing the extendability of kriging models.

5.1.2. Competing models and experiment settings

In order to demonstrate the superiority of the proposed model, we compare SGET with several state-of-the-art baseline methods. These baselines not only contain typical tensor/matrix based spatiotemporal kriging models, but also cover advanced methods from machine learning communities.

- TGMF (Zhang et al., 2020): Temporal geometric matrix factorization. This model uses graph Laplacian and one-order Toeplitz matrix as spatial and temporal regularization. ADMM is used to update variables.
- LSTM-GRMF (Yang et al., 2021): This model extends the graph Laplacian regularized matrix factorization
 framework with LSTM temporal regularization. It can perform online imputation and prediction, while we
 only test the performance of static training and kriging phase.

¹from https://doi.org/10.5281/zenodo.3939793.

²from https://portal.its.pdx.edu/home.

- FMDT-Tucker (Yamamoto et al., 2022): Fast algorithm for multi-way delay embedded (MDT, aka., Hankelization) Tucker decomposition. This work is an enhanced version of Yokota et al. (2018) where the MDT is accelerated by FFT. It utilizes the shift-invariant features of rows/columns to perform image-inpainting which can also achieve spatiotemporal kriging.
- GLTL (Bahadori et al., 2014): Greedy low-rank tensor learning. This is a classical tensor learning method for spatiotemporal kriging and is solved by greedy algorithm.
- **KPMF** (Zhou et al., 2012): Kernelized probabilistic matrix factorization. Row-wise and column-wise kernel(covariance) functions are used as graph side information and a Gaussian process prior is imposed on the factor matrices. This model is solved by stochastic gradient descend method.

In fact, although FMDT-Tucker, GRALS and KPMF are not designed for spatiotemporal kriging in their original works (image inpainting and collaborative filtering), the intrinsic mathematical problems are the same as ours such that they can be transferred to this task. Moreover, BKMF (Lei et al., 2022) and GNNs (Wu et al., 2021a; Liang et al., 2022) are also emerging kriging methods, but we do not include them in the baselines because the Bayesian hyper-parameter sampling procedure in former is time-consuming and the training stage in latter also brings heavy computational burden and memory consumption. Both of them are not well-suited for large-scale problems.

To evaluate the models' performance, a series of observation conditions are tested: we randomly mask the ground truth values of 30%, 50%, 70% locations as unmeasured locations (without sensors), and select 20%, 50% time intervals as unmeasured time (non-operational time). So there are six test scenarios in total, and we name them SM3TM2, SM5TM2, SM5TM5, SM5TM5, SM5TM5, respectively. Furthermore, we also add 20% randomly element-wise missing data to simulate the reality. The performances are evaluated by comparing the estimated values with masked ones. Three evaluation metrics are used in this section: mean absolute error (MAE), they are root mean square error (RMSE) and mean absolute percentage error (MAPE):

$$\begin{aligned} \text{MAE} &= \frac{1}{|\Omega_m|} \sum_{i \in \Omega_m} |x_i - \hat{x}_i|, \\ \text{RMSE} &= \sqrt{\frac{1}{|\Omega_m|} \sum_{i \in \Omega_m} (x_i - \hat{x}_i)^2}, \\ \text{MAPE} &= \frac{1}{|\Omega_m|} \sum_{i \in \Omega_m} |\frac{x_i - \hat{x}_i}{x_i}|, \end{aligned}$$

$$(27)$$

where $\Omega_m = \{(i, j, k) | \text{ when } x_{ijk} \text{ is manually masked and observed data in original tensor} \}$. Detailed hyperparameter settings for SGET and other baselines are given in Appendix A.

5.2. Network-wide kriging results analysis and model comparison

The comparison of kriging performances of SGET and its competing baselines are given in Tab. 3. And we also report the CPU running time of all models on PeMS data in Tab. 4, to show the computation cost.

PeMS-4W (MAE/RMSE) Models SM0.3,TM0.2 SM0.5,TM0.2 SM0.7,TM0.2 SM0.3,TM0.5 SM0.5,TM0.5 SM0.7,TM0.5 **TGMF** 4.49/7.48 4.59/7.61 4.76/7.93 5.16/8.44 6.16/9.19 6.34/9.55 LSTM-GRMF 2.73/5.25 3.25/6.10 3.68/6.91 2.77/4.94 3.39/6.00 3.84/6.90 FMDT-Tucker 4.69/8.39 5.40/9.90 5.88/10.03 4.85/9.05 5.51/10.33 5.91/10.71 **GLTL** 6.07/9.44 6.17/9.59 6.43/9.99 6.08/9.45 6.27 /10.01 6.33/10.08 **KPMF** 4.44 / 7.67 5.05/8.38 6.48/9.63 5.19 /8.44 6.81/10.34 10.28/12.44 SGET 2.61/4.88 3.14/5.68 3.69/**6.59 2.66**/5.04 3.19/5.79 **3.71**/6.63 Portland (MAE/RMSE) Models SM0.3,TM0.2 SM0.5,TM0.2 SM0.7,TM0.2 SM0.3,TM0.5 SM0.5,TM0.5 SM0.7,TM0.5 **TGMF** 5.85/9.58 6.22/9.68 7.38/11.23 5.71/9.57 6.22/9.85 7.50/11.46 LSTM-GRMF 4.57/7.37 3.95/6.82 5.57/8.60 4.10/7.09 4.73/7.41 5.49/8.41 17.03/26.67 14.60/25.01 14.86/23.54 FMDT-Tucker 13.17/19.93 16.75/25.47 14.78/23.04 12.47/18.01 12.14/17.25 12.14/17.45 11.94/16.97 GLTL. 12.27/17.62 12.41/17.90

Table 3: Kriging evaluation on PeMS-4W and Portland data

Best results are bold marked.

5.76/9.11

3.84/6.79

6.14/9.12

4.53/7.29

KPMF

SGET

7.74/10.55

5.39/8.29

4.36/8.00

4.06/7.10

6.51/9.41

4.76/7.41

6.67/9.93

5.56/8.54

Table 4: Running time on PeMS-4W data

Models	PeMS-4W,running time(in second)					
	SM0.3,TM0.2	SM0.5,TM0.2	SM0.7,TM0.2	SM0.3,TM0.5	SM0.5,TM0.5	SM0.7,TM0.5
TGMF	2511.6	2594.5	2739.2	2727.3	2795.1	2844.1
LSTM-GRMF	8965.7	8465.3	8382.2	8172.3	8437.1	8715.3
FMDT-Tucker	2892.8	9311.1	5783.6	4925.3	10902.1	6353.0
GLTL	7408.5	7808.0	6522.9	9673.7	6652.5	6118.5
KPMF	3488.1	1418.4	824.7	2343.9	4918.2	3763.3
SGET	1079.5	1069.7	1081.0	1135.9	1080.8	1090.1

Best results are bold marked.

It can be seen that SGET achieves the highest accuracy in most cases on both of the two datasets. Considering the fact that the datasets we adopt are million-level 'big' data, the superiority of SGET may seem indistinctive compared with LSTM-GRMF. With the decrease of both spatial and temporal observation rates, the performances of all models are degenerated while SGET is supposed to be more robust. Therefore, SGET can achieve networkwide kriging with high accuracy, even though there exists a large proportion of incomplete observations (missing data) in measured locations.

Observing the running time in Tab. 4, we can find that SGET can save more than half the time cost compared to TGMF, which is the most scalable method in the baselines. As discussed in Section 4.5, the computational bottleneck is the updating of graph regularization terms which would introduce large matrix equations, so the room for improvement is limited. Note that KPMF adopts stochastic gradient descent method to update parameters, which is susceptible to local minima, so it could converge to a inferior solution with fewer iteration times. Moreover, LSTM-GRMF also produces competitive performances, especially when TM missing rate is high. Owing to the elaborate LSTM model, it can capture more complex temporal pattern than other models. However, the costs are a lot of training expenses and memory consumption, which are not suitable for network-wide applications. Overall, the proposed SGET achieve state-of-the-art performances in most scenarios, while requires the least computational burden at the same time.

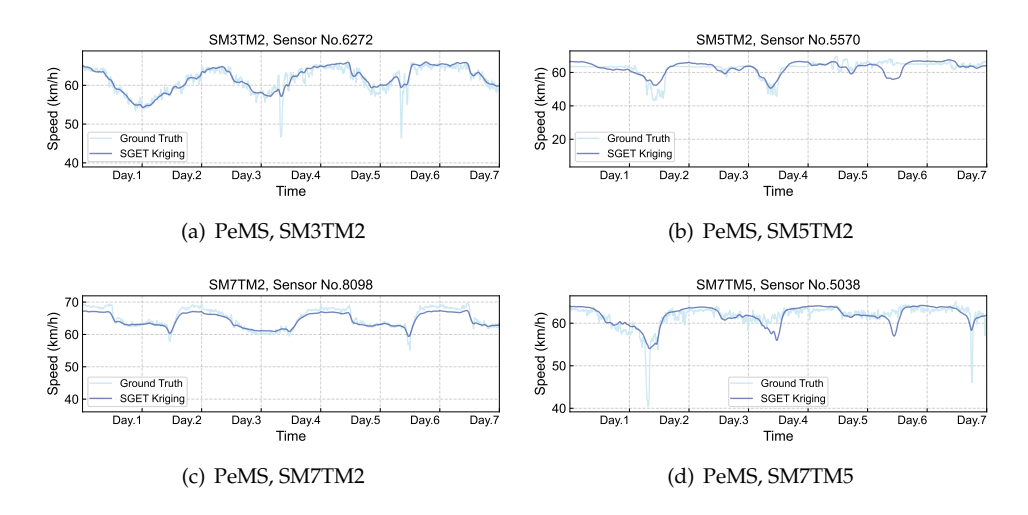


Figure 3: Kriging results visualization for PeMS-4W data. Four randomly selected sensors with different observation conditions are shown. The ground truth values and estimation values are given for comparison.

Furthermore, we give some kriging results on both two data sets in Fig. 3 and 4 to intuitively show the speed estimation performances. Each figure depicts the estimation value and ground truth value for roads randomly selected from unmeasured locations. Overall, SGET estimates accurate time series for unknown locations, even with low observation rate as well as temporal loss. Another facet can be found that SGET produces relatively more smooth signals than the raw data due to the temporal regularization and low-rank condition.

We also give the results of half a day on the first day of PeMS data for detailed comparison in Fig. 5. As can be seen, SGET produces more smooth and stable time series than TGMF and LSTM-GRMF that is closer to the ground truth value. Because there is totally no historical data available, the LSTM model which is widely used to perform time-dimension prediction, is less effective and fluctuates a lot.

The ground truth speed values, SGET and LSTM-GRMF kriging speed values as well as estimation errors of SGET are visualized on the whole California highway network in Fig. 6 (more examples are given in Appendix B.). As we can see, SGET can capture not only the global spatial distributions of traffic speed, but also the speed changes due to local congestion of morning peak. Compared (a), (b) with (c), SGET produces more realistic speed patterns than LSTM-GRMF, which is the best model in the baselines, especially for the local speed changes in

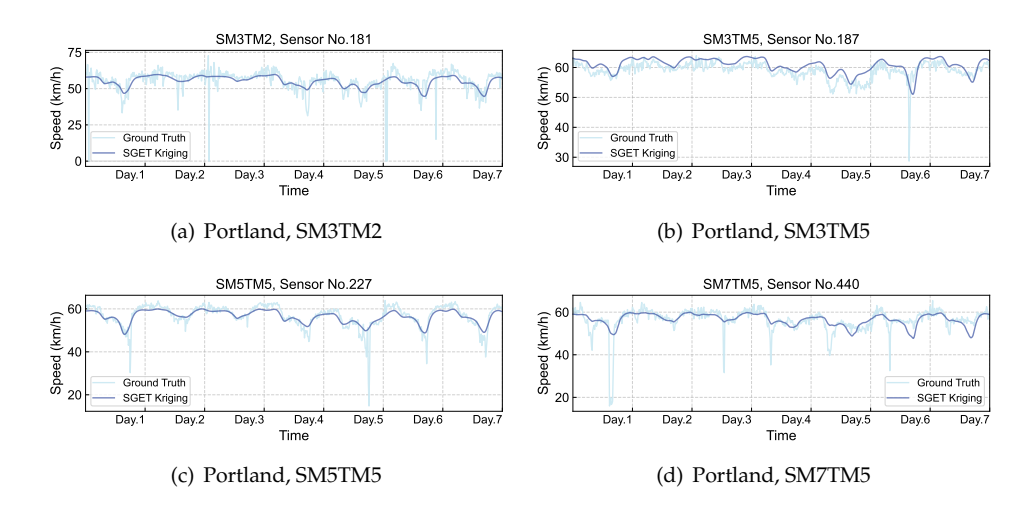


Figure 4: Kriging results visualization for Portland data. Four randomly selected sensors with different observation conditions are shown. The ground truth values and estimation values are given for comparison.

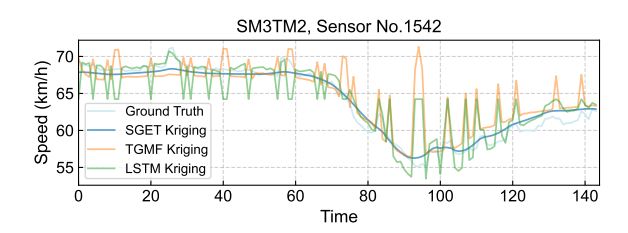


Figure 5: Detailed comparison of different kriging models.

congestion areas. The kriging errors of each link in (d) demonstrate that relatively big errors occur in the areas where there is few or even no neighbor sensors, or congestion districts with drastic changes in traffic speed. As kriging is in fact to aggregate the data of neighbor sensors, the estimation difficulty increases when little referable information is available.

5.3. Algorithmic analysis

5.3.1. Ablation studies

To inspect the significance of each component of the proposed model, in this part we conduct ablation studies to compare the performances of model variations.

- SGET-GFT: We replace the TGFT in our model by the original GFT used in (Deng et al., 2021). To achieve this adjustment, we first transpose the input tensor into shape of (time of day × days × locations) and calculate the graph operator in Eq. (10) by spatial Laplacian. Then, the GFT is performed on the 'location' mode.
- SGET-nRSVD: SGET without randomized SVD. The economic (compact) SVD is used instead.
- SGET-nCG: SGET without conjugate gradient. The matrix equation in Eq. (25) is solved by using the Bartels-Stewart method and this algorithm is achieved by directly calling a package API function scipy. linalg. solve_sylvester(·).
- **SGET-CG iter3** and **SGET-CG iter10**: To test the impact of the numbers of CG inner loops, we set 3 and 10 iterations for implementing Algorithm 3.

We test the above model variations on Portland data and report the resulting performances and running time in Tab. 5. Among these models, SGET with CG iter3 can be viewed as the benchmark. We can find that the kriging accuracy and time cost of SGET-GFT are both inferior. Since the GFT is conducted on the 'location' mode, the tensor SVT needs to be computed a large number of times, which is not cost-effective for network-wide applications. This clearly reveals the effectiveness of the proposed TGFT. What's more, SGET-nRSVD and SGET-nCG are the versions without numeric approximate methods, while their results denote that the numeric accelerating methods in this work, e.g., r-SVD and CG, would not jeopardize the model accuracy, while reducing the computational burden at some degree. Especially, the running time of SGET-nCG is prohibitive, which means that CG plays a key role in kriging scalability.

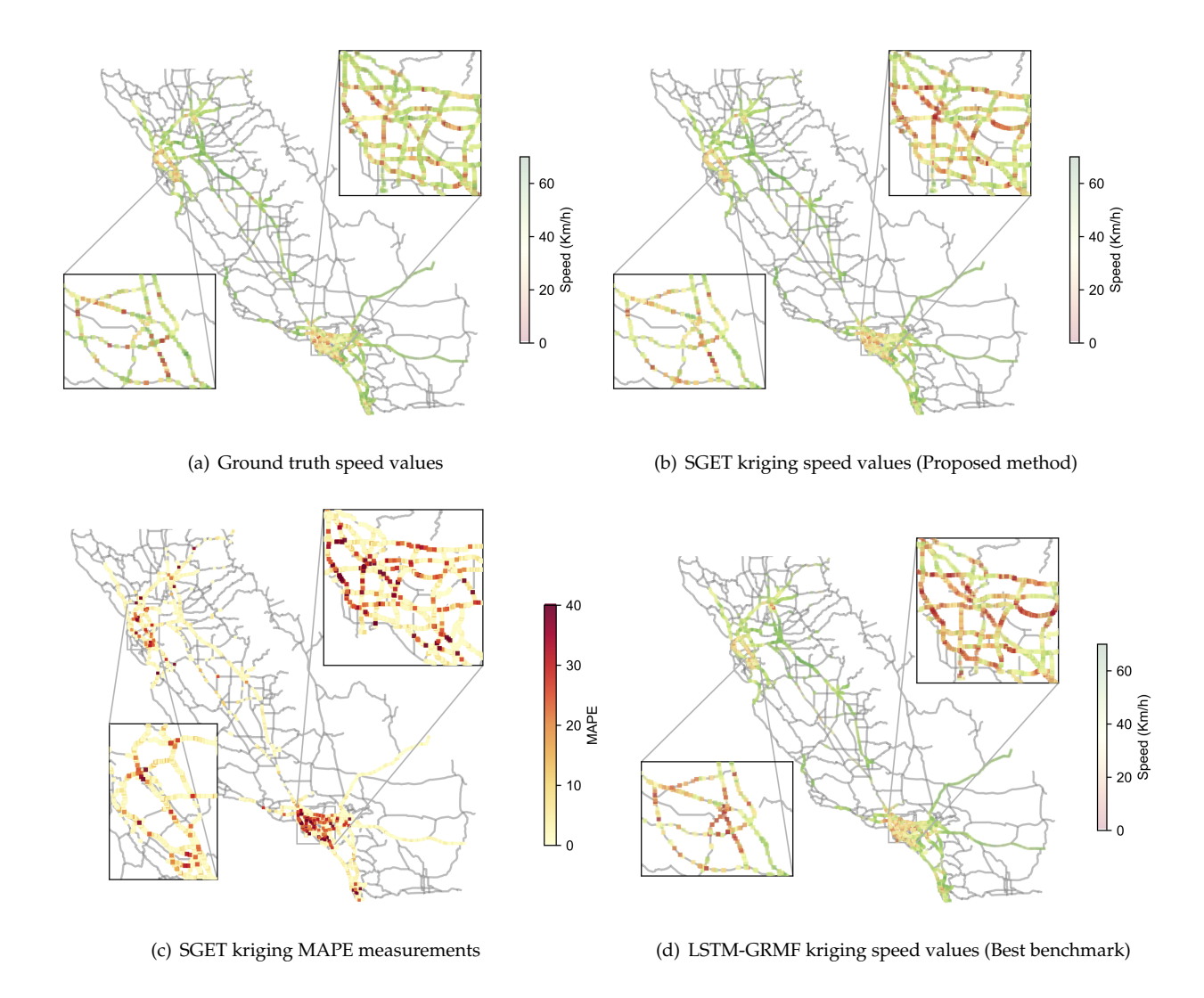


Figure 6: SGET kriging results on the PeMS highway network. Traffic state at 7:00 in the morning is displayed as an example. (a) Ground truth values. (b) SGET estimated traffic speed values. (c) SGET kriging MAPE of each sensor. (d) LSTM-GRMF estimated traffic speed values.

Table 5: Ablation studies

		Portland
Models	MAE/RMSE	Running time (in second)
SGET-GFT SGET-nRSVD SGET-nCG SGET(CG iter3) SGET(CG iter10)	4.76/7.53 4.23/7.02 4.21/7.06 4.21/7.04 4.22/7.04	1100.0 233.7 9107.3 179.5 321.5

By comparing the results of SGET(CG iter3) with SGET(CG iter10), an interesting observation is that the increase of iteration times of CG would not benefit the kriging accuracy in this condition. The underlying reason for this results is that Eq. (26) is highly structure so that CG could convergence with only a few iterations.

5.3.2. Influence of graph partitioning

One significant superiority of SGET is that it can achieve efficient kriging at network-wide and one may wonder why the scalability of kriging model is important from the perspective of algorithmic performance. To demonstrate the necessity and significance of kriging on large-scale data, in this section we conduct experiments on different data size using both of the two datasets. Specifically, we adopt the same graph partitioning method as in (Chen et al., 2021a) to divide the adjacent matrices in $\{1, 2, 4, 8, 16, 32, 64\}$ parts for PeMS data and $\{1, 2, 4, 8, 16, 32\}$ parts for Portland data. The more partitions, the less data scale of each group. In each division case, we conduct kriging on all partitions and record the accuracy and running time of the whole data.

Figs. 7 and 8 show the changes of kriging performances of our SGET and another baseline method TGMF with the increase of graph partitions (decrease of data scales). As can be seen, for both of the two data, the

kriging accuracy of SGET and TGMF decrease remarkably and the best performances are achieved when there is no partitioning. The reasons to explain this phenomenon could be twofold: 1) Previous study (Chen et al., 2021a) has demonstrated that low-rank tensor completion model could achieve better performances on randomly missing data imputation tasks when the data size is large. And in this work, we aim at kriging with incomplete observations and the t-TNN minimization part of our model could benefit from large data scale and learn a better low-rank pattern from a wider range. 2) The spatial graph Laplacian is at the core of kriging model, and it is directly obtained from the network topology structure. When the network is larger, more complicated and comprehensive spatial relations are incorporated in adjacent matrix and the influence of local anomaly can be weakened. Therefore, for unobserved locations there are more informative neighborhoods to provide referable observations when the network is larger.

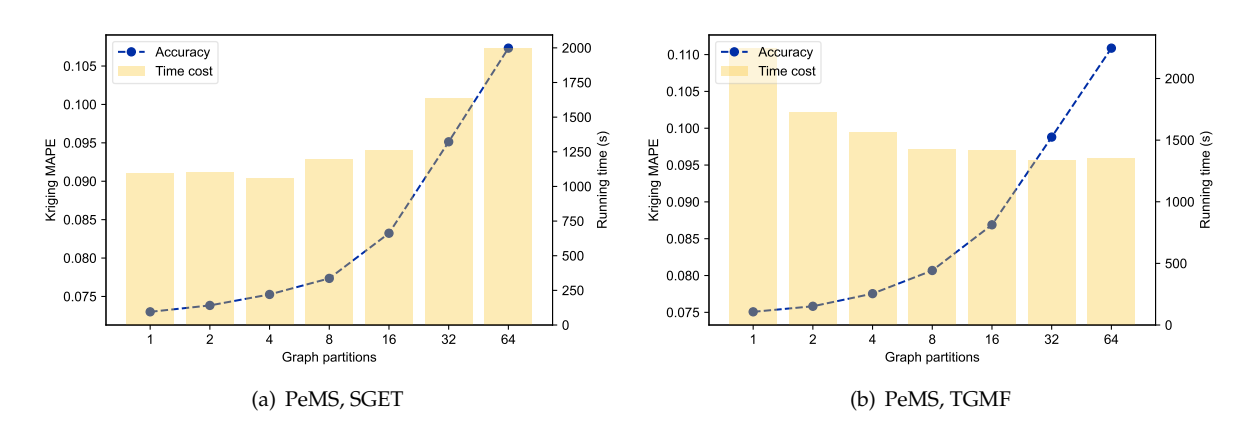


Figure 7: Model performances under different graph partitions on PeMS-4W data. (a) The proposed SGET. (b) TGMF model. The kriging accuracy and running time are both shown in this figure.

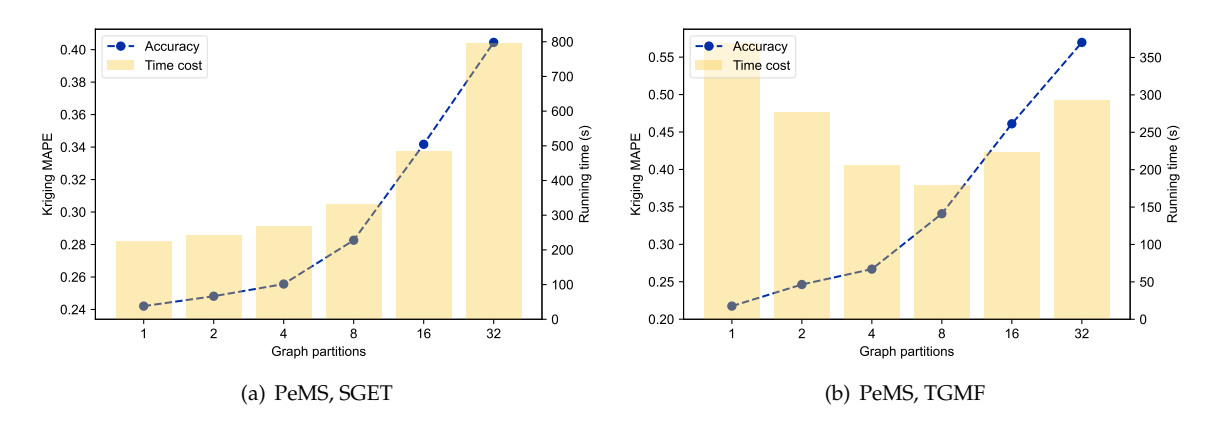


Figure 8: Model performances under different graph partitions on PeMS-4W data. (a) The proposed SGET. (b) TGMF model. The kriging accuracy and running time are both shown in this figure.

Another important observation is that the running time of SGET also gradually increases with more partitions, while the results of TGMF is quite different. Generally speaking, SGET entails the least computation cost when there exists no partitioning while it becomes the largest for TGMF in this situation. This may stem from the reason that SGET can reduce the rank of any arbitrary tensor size in the objective function, but TGMF with a fixed rank settings can not adapt to varying input data size.

Therefore, above results reveal that the proposed SGET that has better kriging scalability than other baseline models is very suitable for large-scale kriging and the motivations behind kriging at network-wide are consideration of both efficiency and precision.

5.3.3. Sensitivity analysis of hyper-parameter

It is generally acknowledged that the hyper-parameter tuning is a long-standing topic in machine learning communities. Most recently, some newly emerged Bayesian hyper-parameter optimization framework has been successfully applied to tensor/matrix factorization models to alleviate this problem (Lei et al., 2022; Chen et al., 2022). However, learning the model hyper-parameters on network-wide data set may be quite difficult. In this work, two main hyper-parameters of SGET that have obvious impact on kriging precision are the regularization factors λ_1 and λ_2 . To discuss about the influence of λ_1 and λ_2 , we examine the model performances under

different parameter settings. Moreover, another potential factor that may affect the sensitivity is the size of input data, we also take it into consideration.

In SGET, the relative magnitudes of λ_1 and λ_2 can make a difference. So we fix $\lambda_1=0.1$ and then set $\rho=\lambda_2/\lambda_1$ as $\{0.01,0.05,0.1,0.5,1,5\}$. We expect to show that the influence of data scale on hyper-parameter sensitivity, so we adopt the same graph partitions on Portland data as in section 5.3.2 and for each partition group we conduct kriging using all six settings of ρ . Note that only the impact of λ_2 is discussed here as λ_2 controls the spatial regularization degree, but similar results can be observed by simply fixing λ_2 and varying λ_1 .

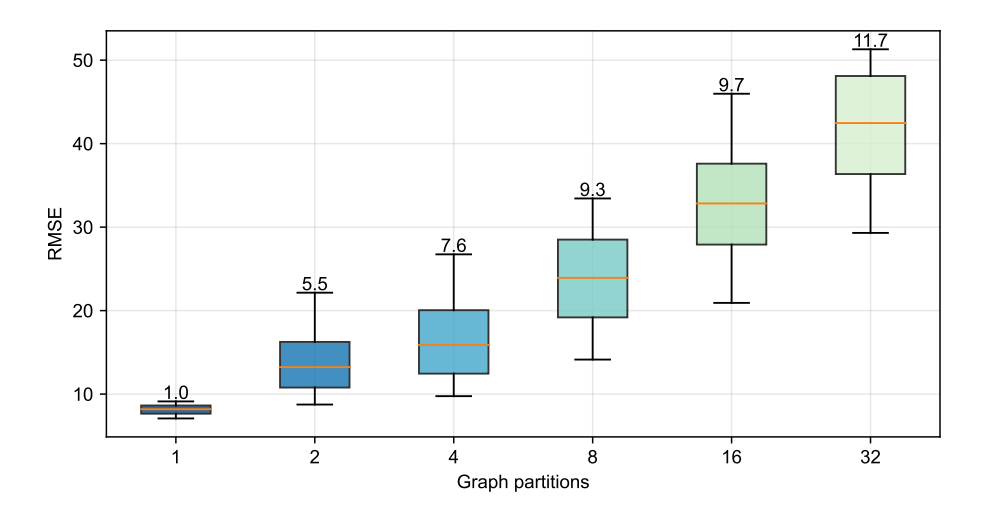


Figure 9: Sensitivity of hyper-parameters under different settings and data scales. The number on the top of each box denotes the IQR.

Fig. 9 gives the box plot for the SGET performances of all ρ setting groups under 6 data scales. Of this figure, each box represents a series of kriging results using different ρ settings on this number of graph partition. We also report the interquartile range (IQR) as a quantitive description, which is defined by the difference between the third and first quartile of each group.

There are two observations from Fig. 9: (1) The RMSE mean value (orange line in this figure) of each group monotonously increases as the partitions increase, and this result is the same as in Section 5.3.2; (2) If we define the IQR as the parameter sensitivity, it is noteworthy that the sensitivity reduces dramatically as the data scale becomes larger and the distance between the upper bound and lower bound of the box also reflects this trend. As a consequence, although we need to specify the model hyper-parameters for SGET without a hyper-parameter learning procedure, we could avoid laborious parameter tuning process on network-wide kriging task because the influence of λ_1 and λ_2 is marginal when kriging on the whole network. In practice, one can obtain the best parameter settings on a small subset of target dataset using cross-validation or grid search techniques and transfer them to the whole data directly, to seek for better model performances.

6. Conclusion and future directions

Sparse sensor coverage and data corruption inhibit availability of fine-grained and network-wide traffic speed data for transportation managements. To cope with this issue, we propose a unified graph embedded tensor (SGET) learning framework which features both low-rankness and multi-dimensional correlations for network-wide traffic speed kriging under limited observations. Three types of speed correlation are carefully chosen: temporal continuity, temporal periodicity, and spatial proximity. Specifically, the temporal periodicity is encoded by a novel temporal graph Fourier transform (TGFT) and thus the tensor nuclear norm minimization problem can be solved in parallel by an array of daily subproblem. To model spatial proximity and temporal continuity for enhancing low-rankness, we adopt spatial graph Laplacian to aggregate available information on graphs and high-order Toeplitz to encourage time smoothness. To further adapt for network-wide data, several efficient numeric techniques such as conjugate gradient (CG) and randomized tensor singular value thresholding (r-tSVT) algorithm are applied to reduce the computational complexity. By performing experiments on two public million-level traffic speed datasets, we draw the following conclusion:

- 1. Our proposed SGET model reconstructs more realistic temporal and spatial patterns of traffic speed than competing models, thereby achieving state-of-the-art kriging performances even with low observation rates, while at the same time saving more than half computing time compared with baseline methods;
- 2. Model ablation studies demonstrate that the approximation algorithms adopted in this work have no negative impact on kriging precision but reduce the computational cost significantly;

3. The sensitivity of SGET hyper-parameters is marginal on large-scale data and can be tuned in an easy routine. Moreover, this work also provides new insights into spatiotemporal traffic data kriging at network level: making fewer efforts to divide dataset could benefit both efficiency and accuracy.

There are some directions worth an extension. First, the model performance is dependent on the calculation of adjacent matrix, where a Gaussian kernel is directly used in this work. It is promising to learn an adaptive adjacent matrix from the raw location information to improve the performance. Second, we only conduct kriging for traffic speed, as the distance based adjacent relationships are practicable for loop speed. However, for trajectory based speed or traffic volume, this assumption may not work. How to achieve accurate kriging for traffic volume is a open question.

Appendix A.

Main hyper-parameter settings for SGET and other baseline models are given as follows: the convergence threshold ϵ for all above models is set to 10^{-3} . For SGET, we set the regularization parameter μ initializing with 10^{-3} and updating in each iteration with $\mu = \min\{1.5 \times \mu, 10^4\}$. The regularization parameters λ_1, λ_2 are selected from cross-validations with $\lambda_1 = 0.001$ and $\lambda_2 = 0.1$. For PeMS data, we set the order of Toeplitz matrix as 1; As Portland data features more complicated temporal mode, we set it to 3 for longer receptive field. For LSTM-GRMF, TGMF and KPMF, a pre-specified rank is necessary, we set it as 60 for Portland data and 200 for PeMS data. For FMDT-Tucker, we set the delay parameter $\tau = [32, 32, 1]$ for Portland and [64, 64, 1] for PeMS. As for GLTL, the orthogonal projection strategy is adopted in these experiments. For both of the two data, we compute the spatial adjacent matrix by Eq. (16). For PeMS data, the distance matrix is based on travel distance, while coordinate position distance is adopted for Portland data.

Appendix B.

Supplementary figures of kriging results on PeMS networks, different time slots from Fig. 6 are given as follows.

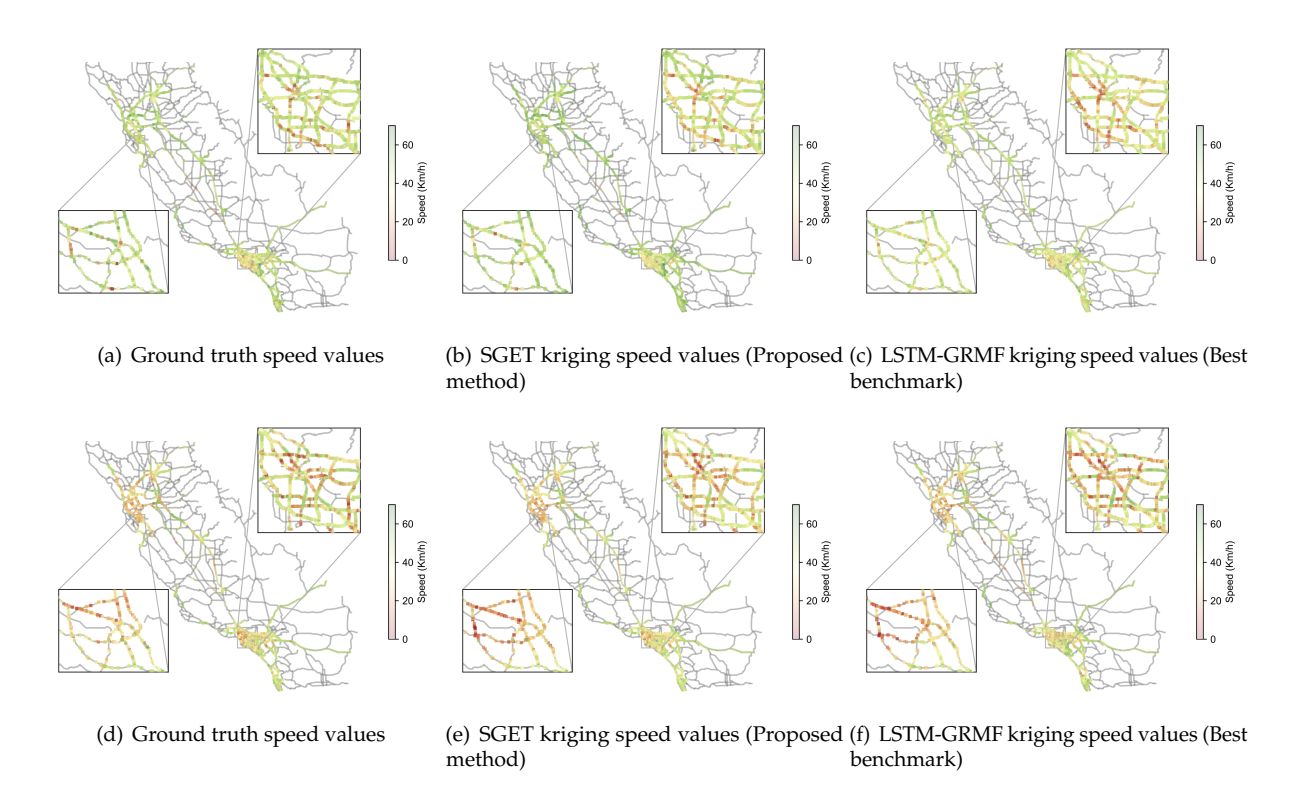


Figure 10: Supplementary figures of kriging results on PeMS networks. Results on two different time slots are plotted.

Acknowledgement

This research was sponsored by the National Natural Science Foundation of China (52125208), and the Science and Technology Commission of Shanghai Municipality (No. 22dz1203200).

References

- Appleby, G., Liu, L., Liu, L.-P., 2020. Kriging convolutional networks. In: Proceedings of the AAAI Conference on Artificial Intelligence. Vol. 34. pp. 3187–3194.
- Asif, M. T., Mitrovic, N., Dauwels, J., Jaillet, P., 2016. Matrix and tensor based methods for missing data estimation in large traffic networks. IEEE Transactions on intelligent transportation systems 17 (7), 1816–1825.
- Bahadori, M. T., Yu, Q. R., Liu, Y., 2014. Fast multivariate spatio-temporal analysis via low rank tensor learning. In: Advances in Neural Information Processing Systems. pp. 3491–3499.
- Boriboonsomsin, K., Barth, M. J., Zhu, W., Vu, A., 2012. Eco-routing navigation system based on multisource historical and real-time traffic information. IEEE Transactions on Intelligent Transportation Systems 13 (4), 1694–1704.
- Chen, X., Chen, Y., Saunier, N., Sun, L., 2021a. Scalable low-rank tensor learning for spatiotemporal traffic data imputation. Transportation Research Part C: Emerging Technologies 129, 103226.
- Chen, X., Lei, M., Saunier, N., Sun, L., 2021b. Low-rank autoregressive tensor completion for spatiotemporal traffic data imputation. IEEE Transactions on Intelligent Transportation Systems, 1–10.
- Chen, Y., Cheng, L., Wu, Y.-C., 2022. Bayesian low-rank matrix completion with dual-graph embedding: Prior analysis and tuning-free inference. arXiv preprint arXiv:2203.10044.
- Deng, L., Liu, X.-Y., Zheng, H., Feng, X., Chen, Y., 2021. Graph spectral regularized tensor completion for traffic data imputation. IEEE Transactions on Intelligent Transportation Systems, 1–15.
- Golub, G. H., Van Loan, C. F., 2013. Matrix computations. JHU press.
- Halko, N., Martinsson, P.-G., Tropp, J. A., 2011. Finding structure with randomness: Probabilistic algorithms for constructing approximate matrix decompositions. SIAM review 53 (2), 217–288.
- Han, X., Shen, G., Yang, X., Kong, X., 2020. Congestion recognition for hybrid urban road systems via digraph convolutional network. Transportation Research Part C: Emerging Technologies 121, 102877.
- Kalofolias, V., Bresson, X., Bronstein, M., Vandergheynst, P., 2014. Matrix completion on graphs. arXiv preprint arXiv:1408.1717.
- Kipf, T. N., Welling, M., 2016. Semi-supervised classification with graph convolutional networks. arXiv preprint arXiv:1609.02907.
- Kolda, T. G., Bader, B. W., 2009. Tensor decompositions and applications. SIAM review 51 (3), 455–500.
- Lei, M., Labbe, A., Wu, Y., Sun, L., 2022. Bayesian kernelized matrix factorization for spatiotemporal traffic data imputation and kriging. IEEE Transactions on Intelligent Transportation Systems, 1–13.
- Li, Y., Yu, R., Shahabi, C., Liu, Y., 2017. Diffusion convolutional recurrent neural network: Data-driven traffic forecasting. arXiv preprint arXiv:1707.01926.
- Liang, W., Li, Y., Xie, K., Zhang, D., Li, K.-C., Souri, A., Li, K., 2022. Spatial-temporal aware inductive graph neural network for c-its data recovery. IEEE Transactions on Intelligent Transportation Systems.
- Liebig, T., Piatkowski, N., Bockermann, C., Morik, K., 2017. Dynamic route planning with real-time traffic predictions. Information Systems 64, 258–265.
- Liu, J., Han, K., Chen, X. M., Ong, G. P., 2019. Spatial-temporal inference of urban traffic emissions based on taxi trajectories and multi-source urban data. Transportation Research Part C: Emerging Technologies 106, 145–165.
- Liu, J., Musialski, P., Wonka, P., Ye, J., 2013. Tensor completion for estimating missing values in visual data. IEEE Transactions on Pattern Analysis and Machine Intelligence 35 (1), 208–220.
- Lu, C., Feng, J., Chen, Y., Liu, W., Lin, Z., Yan, S., 2016. Tensor robust principal component analysis: Exact recovery of corrupted low-rank tensors via convex optimization. In: Proceedings of the IEEE conference on computer vision and pattern recognition. pp. 5249–5257.
- Lu, C., Peng, X., Wei, Y., 2019. Low-rank tensor completion with a new tensor nuclear norm induced by invertible linear transforms. In: Proceedings of the IEEE/CVF Conference on Computer Vision and Pattern Recognition. pp. 5996–6004.

- Luttinen, J., Ilin, A., 2009. Variational gaussian-process factor analysis for modeling spatio-temporal data. Advances in neural information processing systems 22.
- Meng, C., Yi, X., Su, L., Gao, J., Zheng, Y., 2017. City-wide traffic volume inference with loop detector data and taxi trajectories. In: Proceedings of the 25th ACM SIGSPATIAL International Conference on Advances in Geographic Information Systems. pp. 1–10.
- Nie, T., Qin, G., Sun, J., 2022. Truncated tensor schatten p-norm based approach for spatiotemporal traffic data imputation with complicated missing patterns. Transportation Research Part C: Emerging Technologies 141, 103737.
- Rao, N., Yu, H.-F., Ravikumar, P. K., Dhillon, I. S., 2015. Collaborative filtering with graph information: Consistency and scalable methods. Advances in neural information processing systems 28.
- Shi, Q., Yin, J., Cai, J., Cichocki, A., Yokota, T., Chen, L., Yuan, M., Zeng, J., 2020. Block hankel tensor arima for multiple short time series forecasting. In: Proceedings of the AAAI Conference on Artificial Intelligence. Vol. 34. pp. 5758–5766.
- Shuman, D. I., Narang, S. K., Frossard, P., Ortega, A., Vandergheynst, P., 2013. The emerging field of signal processing on graphs: Extending high-dimensional data analysis to networks and other irregular domains. IEEE signal processing magazine 30 (3), 83–98.
- Song, G., Ng, M. K., Zhang, X., 2020. Robust tensor completion using transformed tensor singular value decomposition. Numerical Linear Algebra with Applications 27 (3), e2299.
- Strahl, J., Peltonen, J., Mamitsuka, H., Kaski, S., 2020. Scalable probabilistic matrix factorization with graph-based priors. In: Proceedings of the AAAI Conference on Artificial Intelligence. Vol. 34. pp. 5851–5858.
- Tan, H., Feng, G., Feng, J., Wang, W., Zhang, Y.-J., Li, F., 2013. A tensor-based method for missing traffic data completion. Transportation Research Part C: Emerging Technologies 28, 15–27.
- Wang, X., Miranda-Moreno, L., Sun, L., 2021a. Hankel-structured tensor robust pca for multivariate traffic time series anomaly detection. arXiv preprint arXiv:2110.04352.
- Wang, X., Wu, Y., Zhuang, D., Sun, L., 2021b. Low-rank hankel tensor completion for traffic speed estimation. arXiv preprint arXiv:2105.11335.
- Wang, Y., Zhang, Y., Piao, X., Liu, H., Zhang, K., 2018. Traffic data reconstruction via adaptive spatial-temporal correlations. IEEE Transactions on Intelligent Transportation Systems 20 (4), 1531–1543.
- Wu, Y., Zhuang, D., Labbe, A., Sun, L., 2021a. Inductive graph neural networks for spatiotemporal kriging. In: Proceedings of the AAAI Conference on Artificial Intelligence. Vol. 35. pp. 4478–4485.
- Wu, Y., Zhuang, D., Lei, M., Labbe, A., Sun, L., 2021b. Spatial aggregation and temporal convolution networks for real-time kriging. arXiv preprint arXiv:2109.12144.
- Yamamoto, R., Hontani, H., Imakura, A., Yokota, T., 2022. Fast algorithm for low-rank tensor completion in delay-embedded space. In: Proceedings of the IEEE/CVF Conference on Computer Vision and Pattern Recognition. pp. 2058–2066.
- Yang, J.-M., Peng, Z.-R., Lin, L., 2021. Real-time spatiotemporal prediction and imputation of traffic status based on lstm and graph laplacian regularized matrix factorization. Transportation Research Part C: Emerging Technologies 129, 103228.
- Yang, L., Fang, J., Duan, H., Li, H., Zeng, B., 2018. Fast low-rank bayesian matrix completion with hierarchical gaussian prior models. IEEE Transactions on Signal Processing 66 (11), 2804–2817.
- Yokota, T., Erem, B., Guler, S., Warfield, S. K., Hontani, H., 2018. Missing slice recovery for tensors using a low-rank model in embedded space. In: IEEE Conference on Computer Vision and Pattern Recognition. pp. 8251–8259.
- Yu, H.-F., Rao, N., Dhillon, I. S., 2016. Temporal regularized matrix factorization for high-dimensional time series prediction. Advances in neural information processing systems 29.
- Zhang, Z., Li, M., Lin, X., Wang, Y., 2020. Network-wide traffic flow estimation with insufficient volume detection and crowdsourcing data. Transportation Research Part C: Emerging Technologies 121, 102870.
- Zhou, T., Shan, H., Banerjee, A., Sapiro, G., 2012. Kernelized probabilistic matrix factorization: Exploiting graphs and side information. In: Proceedings of the 2012 SIAM international Conference on Data mining. SIAM, pp. 403–414.